UNIVERSITÀ
DEGLI STUDI
DI PADOVA

DEPARTMENT OF INDUSTRIAL ENGINEERING

**THESIS FOR THE MASTER DEGREE
IN ELECTRICAL ENGINEERING**

INFLUENCE OF CUTTING PROCESS ON MAGNETIC PROPERTIES OF ELECTRICAL STEEL

SUPERVISOR: Prof. Nicola Bianchi
Prof. Antero Arkkio

INSTRUCTOR: Msc. Ugur Aydin

MAJORING: Luca Salvador

ACADEMIC YEAR 2015-16

Abstract

This thesis provides a quantitative analysis of degradation of magnetic properties due to guillotine and laser cutting in non-oriented electrical steel sheets (M270-50A). Rectangular specimens of different widths are cut by guillotine and laser in order to obtain different rate of degradation in the material. The B-H characteristics and losses on these specimens are measured using a custom made Epstein frame under steady state sinusoidal flux density at various frequencies. Measurements results are used to analyse the change in permeability and iron losses. Total measured iron losses are separated into the classical and hysteresis loss components by using least-squares fitting to the well known Jordan model. A finite element model of a 37 kW induction machine is developed and the magnetic characteristics of the damaged and undamaged materials are implemented to the cut edges and the rest of the core material, respectively. Steady state finite elements simulations on the induction machine are performed using FCSMEK, an in-house finite element solver, in order to analyse the effect of material degradation on the losses.

Acknowledgements

This work was carried out at the laboratory of the Department of Electrical Engineering and Automation of Aalto University. The work is part of a research project concerning the losses in electrical machines.

I wish to express my gratitude to my supervisor Professor Antero Arkkio, Head of the Research Group of Electromechanics, for giving me the opportunity to be part of his group of research and using his laboratory for my master's thesis. I am thankful and indebted to my instructor Ugur Aydin for his guidance through all the project and for the time spent to check my work.

I would also like to express my gratitude to Mr. Ari Haavisto, for teaching me to manage the technical resources of the laboratory. A sincere thanks goes also to Professor Anouar Belahcen for his advices about the measurements.

Thanks also to all my colleagues of the Research Group of Electromechanics, for creating a relaxed atmosphere and a good working environment.

Otaniemi, 30.07.16

Luca Salvador

Contents

List of Figures

List of Tables

Symbols and abbreviations

Symbols

$\boldsymbol{B}$	T	Flux Density
$\boldsymbol{H}$	A/m	Field Strength
B_r	T	Remanence
H_c	A/m	Coercive Field
σ	Ω/m^2	Electrical Conductibility
f	Hz	Frequency
p_hy	W/kg	Hysteresis Loss
p_cl	W/kg	Classical Loss
p_ex	W/kg	Excess Loss
ρ	kg/m^3	Density
L_m	m	Magnetic Path

Abbreviations

SST	Single Sheet Tester
nGI	neutron Grating Interferometer
DFI	Dark-field image
DAQ	Data Acquisition Device
NPM	Needle Probe Method
MOKE	Magneto-Optic Kerr-Effect
WEDM	Wire Electrical Discharge Machine

1 Introduction

1.1 Background

The efficiency improvement of rotating electrical machines is driven by two main factors. First, the more and more stringent regulations concerning energy efficiency as the European regulation EC 640/2009 [1] and EC 4/2014 [2] which establish the mandatory energy efficiency class IE3 for the new induction machines. Secondly, the emerging market of electrical and hybrid vehicles that demands motors with high torque density, wide speed range and especially premium efficiency to face the limited capacity of batteries [3].

Design of electrical machines with high efficiency requires increasing accuracy in models for iron-loss estimation. Shortcomings of existing loss models along with lack of knowledge about manufacturing effects give rise to errors in calculated core loss limiting optimization and improvements of efficiency [4]. Manufacturing effects on the losses in electrical machines can be due to cutting, riveting, welding, mechanical stress and packet assembling [5].

It is well-known that the losses in electrical machines are affected by these processing techniques therefore they are usually considered during design by building factors. These corrective coefficients have intrinsic limitations due to the simplification adopted to represent complex phenomenons with few parameters. Therefore, nowadays better ways to describe influence of building processes are studied.

Main manufacturing process during building of electrical machine is the cutting of laminations to build the core of the machine. During this operation, according to the method used, the tool affects the properties of the core material [6]. Influence can be really important at the point that annealing is compulsory to limit degradation effect [7].

Principal cutting techniques used in building of electrical machines are punching, used mainly for big series machine because the low cost and high speed, and laser or water-jet cutting techniques are slower but more flexible and used mainly for small series.

1.2 Objectives of Thesis

The thesis aims to investigate the effects of cutting process on the permeability and on the iron losses in ferromagnetic materials. Effects of guillotine and laser cutting are studied and compared within a wide range of frequency and flux density.

A grade M270-50A non-oriented electrical steel sheet with 3% Si content is cut into rectangular strips with different widths using the afore mentioned cutting methods and magnetic characteristics of the specimens are measured using a custom made Epstein frame. The experiments give an idea of how the permeability and losses are affected and at which rates.

Then finite element analysis on a 37 kW induction machine is performed using damaged material properties at the cut edges in order to study the influence of cutting on the losses of the studied rotating electrical machine.

The project is divided into the following tasks:

- Perform experimental measurements on electrical steel samples to evaluate the effects of the cutting process on the magnetic properties of the material, this task is composed by three subtasks:
  - Adjusting the measurement setup in order to couple it to a custom made Epstein frame.
  - Build a mutual inductor to eliminate the flux leakage in the Epstein frame.
  - Measuring the B-H curves of the specimens which have different widths and cut by guillotine or laser under various frequencies. Afterwards, calculating the permeabilities and specific losses using the measured B-H curves of each case.
- Quantifying the effect of cutting on the specific losses and permeability and compare results from guillotine cut samples with laser cut ones.
- Using experimental results to perform a finite element method simulation and quantify the effects of cutting in an electrical machine.
- Evaluating the results obtained answering to the following questions:
  - Which method influences the magnetic properties of the material the most?
  - Which loss component is influenced the most?
  - How much is the rate of influence on the loss of the studied electrical machine?

1.3 Thesis Outline

- **Chapter 2**: Relation between the structure of the material and the magnetic properties focusing on the loss behaviour and components. Models used in literature to describe losses mechanisms in the ferromagnetic materials.
- **Chapter 3**: Main measurement techniques that are used to study degradation of magnetic properties in electrical steels.
- **Chapter 4**: Brief introduction of the main cutting techniques. Effects that these techniques cause in electrical steels according to the literature. Comparison of literature's results obtained from different methods of measurements.
- **Chapter 5**: Description of the performed experiment, starting from the presentation of all the devices used for the measurements, passing to the explanation of the procedure used to obtain the results.
- **Chapter 6**: Report of the more representative measurement results through graphs and comparative tables.

- **Chapter 7**: Comparison between mechanical and laser cut measurements, numerical processing of the data with finite elements method and comments about final results obtained by simulation on a 37 kW induction machine.
- **Chapter 8**: Conclusion about the results, critical assessment about the experiment and feasible improvements. Some proposals about the future works to integrate the measurements and obtain further results.

2 Ferromagnetic Materials

Ferromagnetic materials are characterized by a particular magnetization curve, due to the relation between structure of lattice and magnetic domains. In particular magnetic domains contribute to magnetization at low flux density and at the same time generate losses in the material. In this chapter the relations among microstructure of ferromagnetic material, losses and magnetization are presented. Then the influence of cutting on the magnetic behaviour is explained.

2.1 Magnetization of Magnetic Domains

Ferromagnetic materials produce elevate value of magnetic polarization ($\boldsymbol{P}$) when are crossed by a field strength ($\boldsymbol{H}$). This characteristic makes ferromagnetic materials suitable for generation of high flux density in electrical machine, necessary to create torque.

The structure of these materials is constituted by magnetic-domains, in each domain all the magnetic dipole moments point in the same direction therefore, we can say that each domain behaves like a permanent magnet with maximum value of polarization (value of saturation).

The zone between two magnetic domains is called domain wall, it behaves like a transition area between two domains with different direction of polarization. If the domain walls are not magnetized they are disposed in configuration of minimum energy.

When the material is magnetized with a quasi-static process the domain walls relocate themselves in a new configuration to find a new equilibrium between forces applied by the domains and the magnetic moments produced by magnetic field. The passage to a new equilibrium is not continuous, because impurities and imperfections in the lattice of the material pin the domain walls which tend to jump between a configuration of local minimum to another one displacing from subsequent pinning points [8]. The jump between two pinning points is called Barkhausen jump and is the cause of hysteresis loss.

When higher field strength is applied domain walls start to disappear and magnetic dipole moments gradually rotate until in all domains the dipoles get the same direction, see Figure 1 [4].

Manufacturing processes influence grains of material which can cause new imperfections in the lattice and then new pinning sites for the domain walls. At the same time stresses induced in the material displace the lattice hindering the magnetization process of the damaged zone, and making the cut edge harder to magnetize [9]. These changes are more relevant with low flux density when magnetisation is influenced by wall domain displacing while loses importance as soon as the rotation of magnetic dipoles becomes the main cause of the polarization.

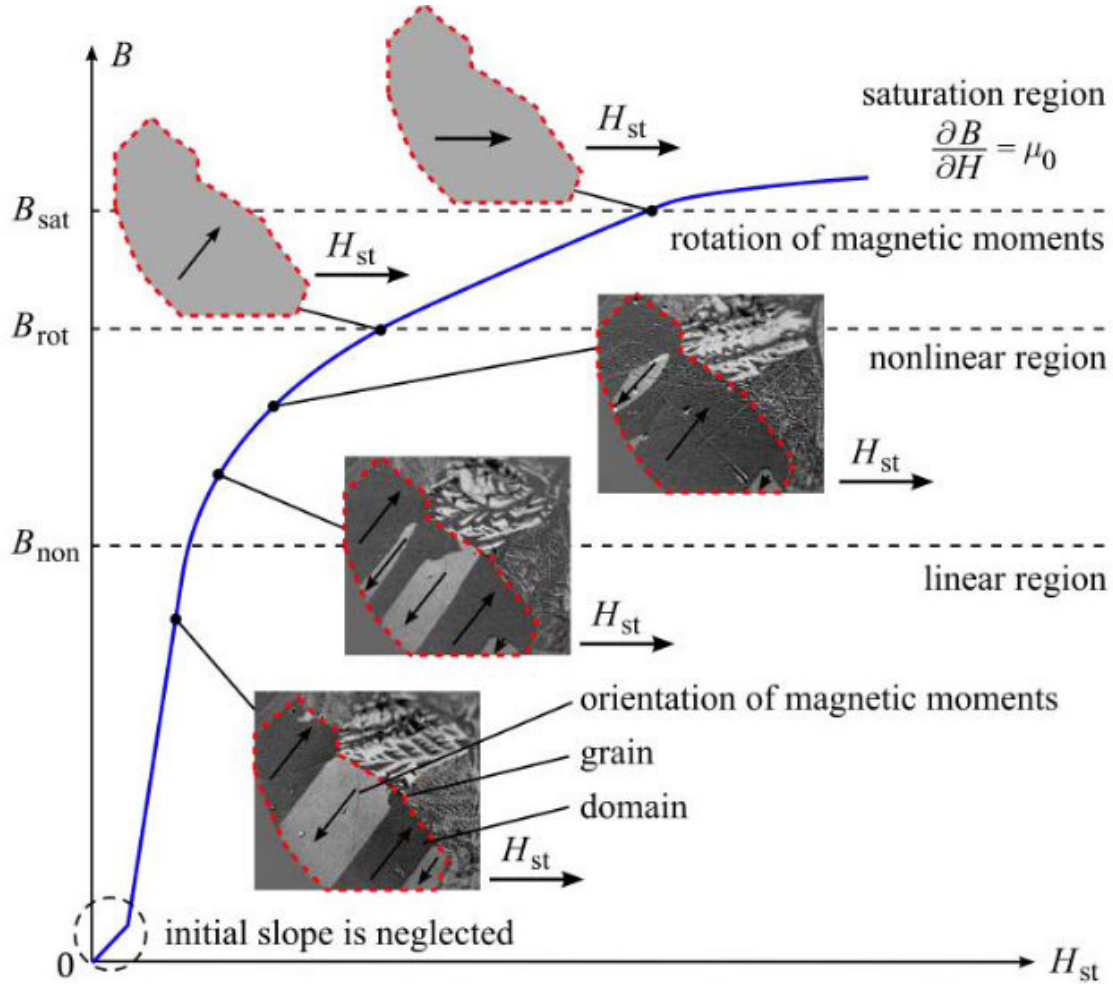

Figure 1: Relation between magnetization curve, magnetic domains and magnetic moments [4].

2.2 Loss Components

The losses of rotating electrical machines are composed mainly of resistive losses in the windings and iron losses due to variable flux in magnetic path of the core. The iron losses can be divided in three components: hysteresis, classical and excess loss. In this section each component will be presented and the relation with degradation provoked by cutting will be analysed.

2.2.1 Hysteresis Loss

It has been already shown how magnetization evolves in a quasi-static process, see Figure 1. In that case, Barkhausen jumps provoke rapid micro movements of domain walls which induce micro eddy currents. The joule effect caused by these eddy currents is called hysteresis loss (p_{hy}) and corresponds to the value of loss in the quasi-static state. Micro eddy currents are located on the edge of domains, therefore bigger size of grains and then wider magnetic domains bring lower loss [12], [14].

Moreover, hysteresis energy loss is independent from frequency and hysteresis power loss is a linear function of the frequency depends only on peak flux density while is independent of wave-shape of **B** [10]–[13].

During experiments only one power measurement is needed to know hysteresis loss for all frequencies. By the way measuring loss in quasi-static state is not always possible and interpolation of some measurements at low frequency should be preferred.

Because the independence with frequency of loss per cycle, when frequency increases beyond hundreds of hertz hysteresis loss is usually small compared with the others components which rise with frequency.

Consequently, hysteresis energy loss depends from peak flux, structure of material and density of pinning sites. For this reason process of cutting on the material that affect structure of steel can rise this loss component.

2.2.2 Classical Loss

During dynamic magnetization macroscopic eddy currents are produced by field strength induced in the material, according to Maxwell's laws. The joule effect produced by these eddy currents is called classical loss (p_{cl}). This component can be obtained either by interpolation of experimental measurements or can be calculated in a strip by Formulation 1 under some assumptions as homogeneous material, uniform and sinusoidal magnetic field, no skin effect, no rotational fields [15]:

$$p_{\mathrm{cl}} = \frac{\pi^2 d^2 \sigma (Bf)^2}{6\rho} \tag{1}$$

where σ is the electrical conductivity of the material, d the lamination thickness, f the frequency and B the peak value of flux density. From Formulation 1 we observe that in order to reduce this component one way is to increase the specific resistivity of the iron, an other way is reducing the thickness (d) of the laminations.

Cutting might alter the resistivity of the material only in few μm next to the cut edge so the classical loss should not be directly influenced by cutting processes and usually the variation is not taken into account [10], [16], [17]. However, the change of permeability due to cutting leads higher and lower flux densities in undamaged and damaged parts of material, respectively when the total flux is kept constant. As shown in Figure 2, this effect causes flux to focus in a smaller area resulting eddy current path to become shorter. This phenomenon reduces classical loss but the change is negligible until the thickness of the lamination sheet is much smaller than the width [10].

2.2.3 Excess Loss

The last term considered to study iron loss is called excess loss (p_{ex}). Like the hysteresis loss the source of excess loss is the micro eddy currents generated by Barkhausen jumps, but in this case dynamic magnetization is considered and the relation with time and speed of jumps affects this loss.

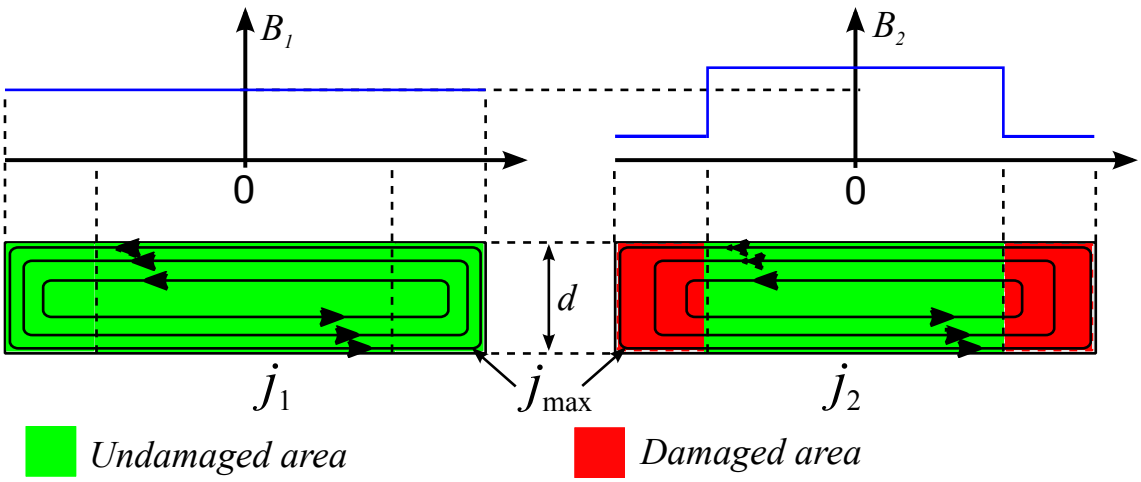

Figure 2: Eddy current (black arrows) in a strip for same average value of flux but different distribution [10].

Differently from classical loss, there is not theoretical formulation for this component. Consequently, experimental measurements are needed to obtain the curve of loss for all frequencies.

Also the excess loss like hysteresis component is influenced by micro-structure of steel and density of pinning sites, so it is expected that cutting process that damage the material influence the excess loss component, further influence of frequency should be visible.

It is worth mentioning that the classical and excess losses together are called dynamic loss (p_{dy}) in opposition with hysteresis component where quasi-static state is considered.

2.3 Loss Models

In previous section physical reasons for iron losses are explained. However quantifying losses studying magnetic domains is complex, moreover when the aim is to design an electrical machine we are more interested in macroscopic effects in the whole. Therefore, some empirical models have been developed to obtain iron losses in a large range of flux density and frequency with few measurements of material. In this section some models for iron loss calculation are presented.

2.3.1 Steinmetz Equation

Steinmetz equation describe losses in iron with a single component [18]:

$$p_{\mathrm{fe}} = C_{\mathrm{st}} B^{\alpha} f^{\beta} \tag{2}$$

where B is the peak value of the flux density, f is the frequency of the sinusoidal flux and the three coefficients C_{st}, α and β depend on the material and can be obtained by fitting to experimental results. This model assumes a sinusoidal flux, so using it for high flux density above knee of saturation may lead to inaccurate results. The range

of frequency where the calculated values are accurate is small and it is suggested to calculate the coefficients for different frequency range to avoid a discrepancy too high between calculated and measured values [19]. Because of the non-linearity of the formulation it is not possible to use a linear system to calculate the coefficients.

2.3.2 Modified Steinmetz Equation

Because the shortcomings of the Steinmetz equation some improvements on previous formulation were proposed. One of this is the modified Steinmetz equation which works also with non-sinusoidal flux:

$$p_{\mathrm{fe}} = C_{\mathrm{st}} B^{\alpha} f_{\mathrm{eq}}^{\beta-1} f \tag{3}$$

where f_{eq} is the equivalent frequency that takes into account variation of flux density in time-domain [8]. To calculate f_{eq} the flux density as function of time is needed. A further formulation based on Steinmetz equation is presented in [20].

2.3.3 Jordan Equation

Jordan Equation divides power loss into two components, hysteresis and classical losses:

$$p_{\mathrm{fe}} = p_{\mathrm{hy}} + p_{\mathrm{cl}} = C_{\mathrm{hy}} B^2 f + C_{\mathrm{cl}} B^2 f^2 \tag{4}$$

where hysteresis component is proportional to the frequency and is the dominant term with $f \to 0$ while the second component so called dynamic component is proportional to the second power of the frequency. The loss coefficient C_{cl} can be found by using experimental data or using the expression:

$$C_{\mathrm{cl}} = \frac{\pi^2 d^2 \sigma}{6\rho} \tag{5}$$

where d is the thickness of lamination, ρ is the material density and σ the conductivity. A linear system with data from different measurements can be used to calculate the coefficients thanks to linearity between B^2 and $B^2 f^2$ [19]. However, the Equation 5 shows inaccuracy between different electrical steel alloys and therefore has been improved successively to consider the difference between some materials, see Equation 6.

2.3.4 Pry and Bean Equation

Pry and Bean equation is derived from Jordan equation but present a further coefficient that is material dependent:

$$p_{\mathrm{fe}} = p_{\mathrm{hy}} + p_{\mathrm{cl}} = C_{\mathrm{hy}} B^2 f + \eta_{\mathrm{ex}} C_{\mathrm{cl}} B^2 f^2 \tag{6}$$

where η_{ex} is defined as excess loss factor and is evaluated by experimental values between different materials. As for Jordan equation also these coefficients can be obtained by a linear system [19].

2.3.5 Bertotti Equation

Bertotti introduces the excess loss based on a statistical approach developed considering the magnetic objects, i.e. a group of similar magnetic domains [11], [12], [21]. The equation developed is:

$$p_{\mathrm{fe}} = p_{\mathrm{hy}} + p_{\mathrm{cl}} + p_{\mathrm{ex}} = C_{\mathrm{hy}} B^2 f + C_{\mathrm{cl}} B^2 f^2 + C_{\mathrm{ex}} B^{1.5} f^{1.5} \tag{7}$$

This formulation is more precise at high frequency where the third term becomes relevant.

2.3.6 Rotational Field loss

Some parts of electrical machines like intersections between teeth and yoke are exposed to rotational magnetization which induces a different behaviour of loss. To take into account this parameter further formulations are developed in [22]:

$$p_{\mathrm{fe}} = C_{\mathrm{hy}} \left(1 + \frac{B_{\mathrm{min}}}{B_{\mathrm{max}}} (r - 1) \right) B^2 f + (C_{\mathrm{dy1}} + C_{\mathrm{dy2}} B^{\alpha}) B^2 f^2 \tag{8}$$

where r is the rotational hysteresis factor while C_{dy1} and C_{dy2} are two dynamic loss coefficients introduced to have a more accurate results at high flux density thanks to a high order term.

In [19] it is shown that the coefficients of the model are strongly influenced by range of frequency and range of flux density chosen for interpolation. Therefore, attention should be paid about the range of measurements used in the fitting process.

2.4 Electrical Steel

The ferromagnetic materials commonly used for the building of core in rotating electrical machines are called electrical steel. It is usually constituted by silicon-iron alloys (FeSi) but also nickel-iron (NiFe) and cobalt-iron (CoFe) are used for high performance machines. These alloys have high magnetic permeability and low iron loss. The percentage of silicon is variable from 2 to 3,5%. A higher silicon percentage increases size of grains during production of alloy reducing loss, at the same time increasing resistivity reducing eddy current [23]. However it also reduces workability of the material making building of machine more difficult.

The material is usually laminated with thicknesses varying from 0,1 to 1 mm. Non-oriented steel are generally used, especially in medium and small machines where the whole stator is obtained from a single sheet and an as isotropic as possible material is preferred. To obtain the fully-processed steel the sheets are usually annealed, cleaned, smoothed and coated with a thin layer of insulating.

Electrical steels are commonly classified according loss at 50 Hz and 1,5 T. The guaranteed values on the datasheet are obtained by standard measurements by means of an Epstein frame. The width of the samples sheets for Epstein frame is 30 mm, therefore if an electrical machine is to be studied with cutting effects the datasheet values might not be suitable since there might be regions where the width of the core

material is less than 30 mm for instance, teeth width in small and medium machines. Therefore, measurements with smaller sample width might be needed.

2.5 Summary

In this chapter an overview about ferromagnetic materials is introduced to understand how cutting process can influence magnetic properties, in particular:

- How the process of magnetization is influenced by deformation of grains induced by cutting.
- Why the three components of iron losses increase with degradation induced by cutting.
- Loss models developed to describe components of loss in ferromagnetic material are also presented.
- Finally brief presentation of electrical steel used in constructing of rotating electrical machines.

3 Measurement Techniques

Controversial results are found on literature about influence of cutting process in the material. In particular the depth of degradation inside the material is much discussed and there are not uniform results. It is observed that the results change with different measurement techniques. For this reason, in the next chapter we will present the common methods used to study degradation in the ferromagnetic materials trying to understand the different results obtained. The methods are divided in direct and indirect methods.

3.1 Indirect Methods

Indirect methods or induction methods are based on the Faraday's law. The approach is to force a periodical field strength that generates a magnetic flux through a closed magnetic path constituted by the sample. The average field strength obtained by one or more excitation coils wound around the specimen can be calculated after measuring current on the excitation coil, according Equation 9. The average flux density can be calculated after measurements of induced voltage by an unloaded search coil wound around the specimen by using Equation 10.

The relation between the field strength and the induced flux density is dependent to the properties of the sample. Therefore the permeability of the sample can be calculated. The specific loss generated in the magnetic path can be calculated knowing the density of material and cross section of the flux path through the Equation 11.

$$H_{\text{ex}} = \frac{N_{\text{ex}}}{L_{\text{m}}} i_{\text{ex}} \tag{9}$$

$$B_{\text{in}} = \frac{1}{N_{\text{s}} S} \int_T v_{\text{sc}}\, dt \tag{10}$$

$$p = \frac{1}{\rho T} \int_T H_{\text{ex}} \frac{dB_{\text{in}}}{dt} dt \tag{11}$$

In the formulations above N_{ex} and N_{s} are the number of turns of exciting coil and search coil respectively, i_{ex} the current in excitation coil, v_{s} the voltage of the search coil, ρ is the density of material, T is the period, S the cross section of the magnetic path and L_{m} the length of the magnetic path. The equations above are verified until the flux can be assumed constant along all the sample and in sinusoidal steady state, S is assumed constant and the flux leakage is negligible.

The most known experimental test setups where induction method is used in order to study the degradation in electrical steel are Epstein frame, single sheet tester, toroid test and stator test.

3.1.1 Epstein Frame

Epstein frame is one of the standard method presented in IEC for certification of power loss and BH curve in ferromagnetic materials [24]. In the standards this

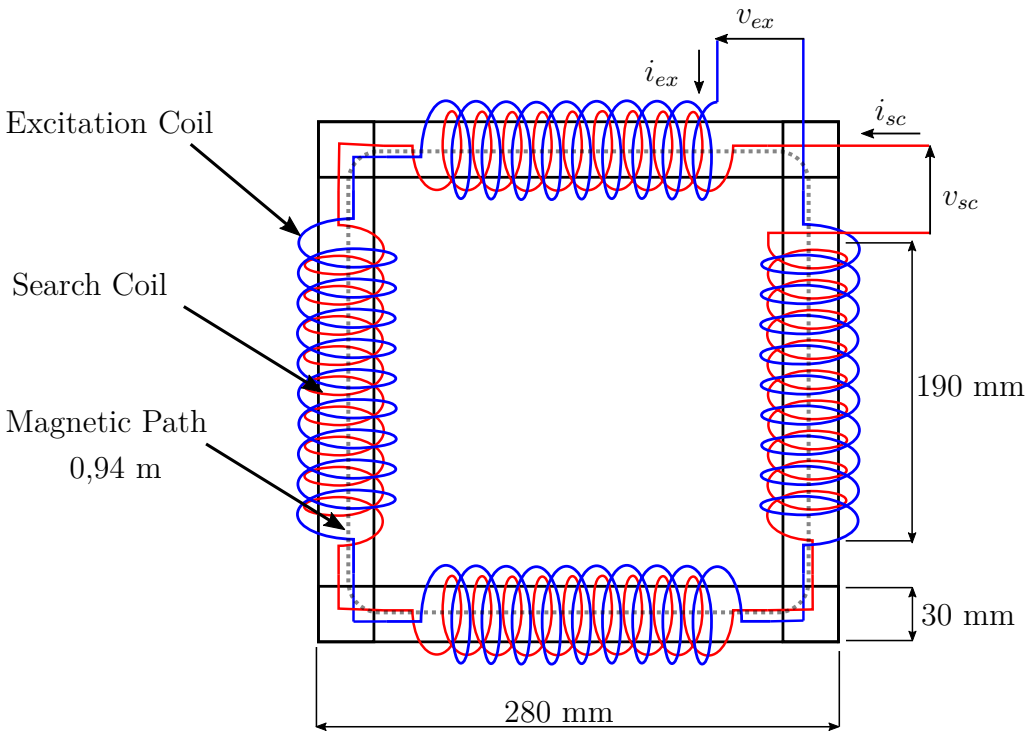

Figure 3: Simplified scheme of Epstein Frame formed by four excitation coils in series connected to the power supply and four search coils in series unloaded. In grey the approximate magnetic path.

method is presented for magnetic flux in sinusoidal steady state. The geometry of samples and tolerance of each component are fixed to ensure reproducibility of results. In the standards this method is presented for magnetic flux in sinusoidal steady state. Magnetic flux must be maintained sinusoidal within a maximum deviation of form factor [24]. The frame is composed by four excitation coils in series connected to the power supply which form the primary winding and four search coils in series unloaded which constitute the secondary winding. Specimens are allocated on the frame forming a closed squared path as shown in Figure 3.

When high field strength is induced and the material gets in deep saturation a feedback control is needed to maintain the form factor of B-field. Moreover voltage and current become in quadrature ($\cos\varphi \to 0$) because the high current of magnetization is supplied and elevated reactive power brings intrinsic inaccuracy in calculation of active power [26], [27]. In this case thermometric method can substitute the Epstein frame as it measures only active power and is not influenced by low power factor [25].

The grade of degradation can be obtained comparing strips with different width, i.e. different density of damaged material. In this way it is possible to find the relation between the depth of degradation, drop of permeability and rise in losses without measuring the local flux density close to the cut edge. Preparation of samples is usually time-consuming because strips of different width have to be cut. However specimens are simple strips which are not difficult to obtain. The limit of this approach is the difficulty to obtain very narrow strips and usually strips smaller

than 4-5 mm are not studied. This constraint set the minimum depth that can be analysed with this method.

3.1.2 Single Sheet Tester

Single Sheet Tester (SST) is a IEC standard method for certification of power loss and BH curve in ferromagnetic materials [28]. The principles of this method are the same of Epstein frame, excitation coil and search coil are wound up around the specimen, two U-shape magnetic paths close the path.

Compared to the Epstein frame the preparation of samples is easier and less number of specimens are needed. Voltage and current measurements can be used or also a fluxmeter can measure directly the H-field to avoid calculating the length of magnetic path (L_{m}) that can be subjected to errors [29]. For certification of loss usually calibration by Epstein frame is done to set the length of path. [30].

The degradation is obtained comparing the results from strips of different width.

3.1.3 Toroid Test

Toroid test works with the same principle of the Epstein frame but the magnetic path is constituted by ring specimens stacked together to obtain a toroid as shown in Figure 4 [31]. Windings have to be wound around for each specimen and therefore, this method is more time-consuming if we have to measure several samples. A further difficulty is that the ring shape of the samples can not be obtained by guillotine.

Toroidal core provides a better representation of magnetic path in a rotating electrical machine because of the similar geometry to the stator. Moreover, the flux is more uniform without any air gap along the magnetic path and therefore, toroid test can be more accurate of Epstein frame and usually shows higher loss [30].

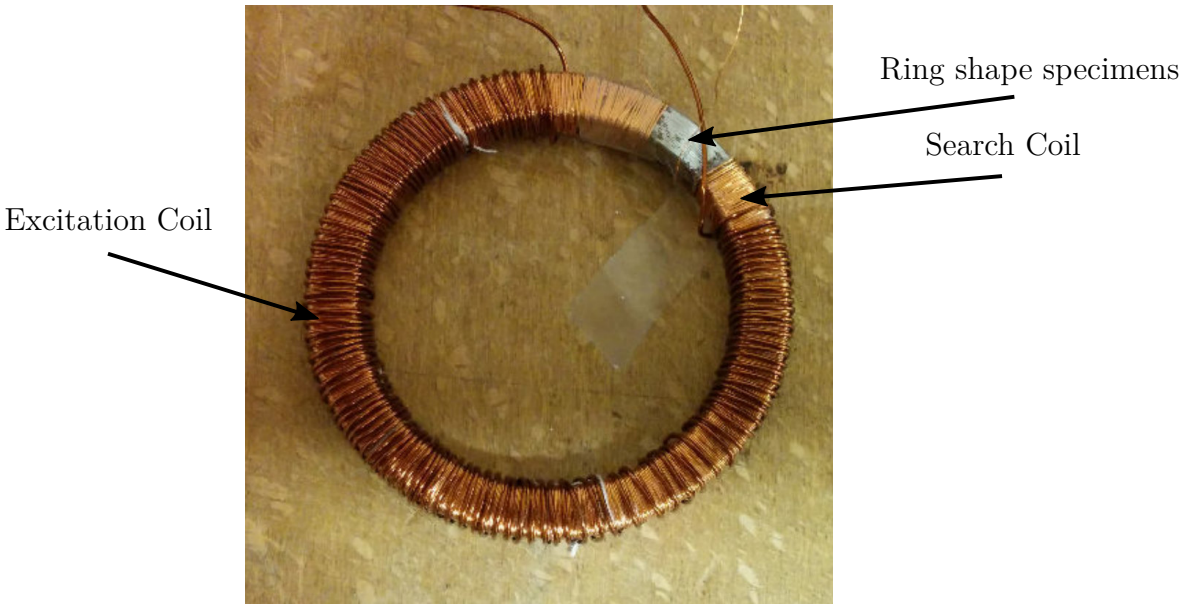

Figure 4: Toroid Test [31].

If depth of degradation is needed to be studied by using toroid test, many rings with different diameter need to prepared which makes this method ineffective for this study purpose.

3.1.4 Stator Test

In Stator Test the magnetic path is constituted by sheets of stator which have to be stacked and wound up. In particular search coils must be wound in the slots between the teeth to measure the flux in the yoke, see Figure 5 [31]. Stator specimens have same shape of stator therefore, evaluation of cutting effects in rotating electrical machine is optimal.

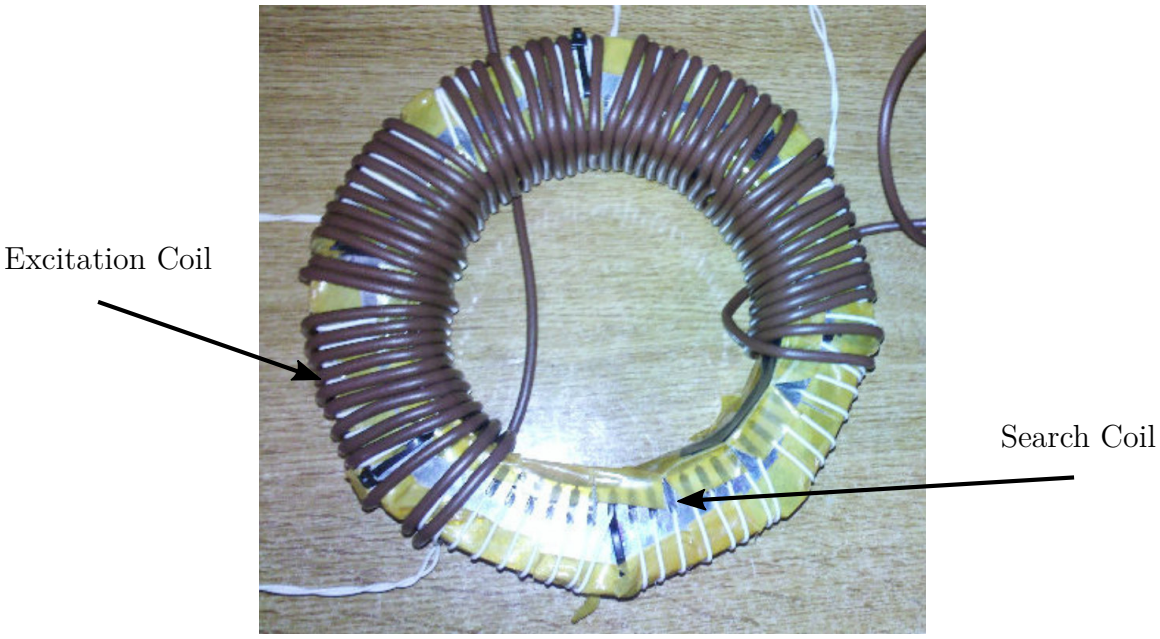

Figure 5: Stator Test [31].

3.2 Direct Methods

Direct methods permit to obtain measurements in specific spots of the specimen, it is possible to study local magnetic properties in the damaged area. Some of the direct methods that can be used to detect degradation due to cutting are the Search Coils, the Needle Probe method, The Dark Field Image method and the Local Magnetic contrast.

3.2.1 Search Coils

Search coils is a destructive method that uses the same principle of SST, but in this case several search coils are positioned in different parts of the sample to measure the local field in degraded area of the specimen. The coils are wound up through the specimen usually after some holes are drilled in the sample. On the one hand it is possible obtain the flux density distribution with a high measurements for area of specimen along all the width of the strip. On the other hand many holes in the strip can damage further the material affecting also the measurements [4], [10], [32]. It is not necessary to have narrow strips and drilling the sample is quicker than cutting strips of different width.

3.2.2 Needle Probe Method

Needle probe method (NPM) is a non-destructive method that permit to calculate the local flux density forcing a field strength in the specimen. Needle probes are positioned in different spots on the surface of the specimen. Applying Faraday's law between the different potentials measured by probes it is possible calculating the local flux density. The needles placed on the surface do not modify the material properties. Measurements need to be corrected by a time-consuming numerical procedure to eliminate the inaccuracy and noise of probes [10]. Moreover, measurements of all sample with indirect methods are still necessary to have a reference for needle probe method measurements.

Disadvantages of needle probe method are error due to vertical electric field component, sensitivity to noise interference, the necessary evaluation of the coating on the sample [34]. However, needle probes can be located very close to the surface so number of measurements for area of specimen is high.

3.2.3 Dark Field Image Method

Dark Field Image (DFI) is a direct non-destructive method to observe the local changes in the magnetic flux density inside the material. The measurement system is composed by a neutron beam source, a neutron grating interferometer (nGI) formed by three different layers, a source grating, a phase grating and an analyser grating, at the end of the beam path a detector of neutron beam is collocated.

The specimen is put on the nGI and a neutron beam passes through the sample. Local changes in the oscillation of the signal intensity are induced by the neutron interaction with domain walls, where the changes of direction of the magnetization

resulting in a refraction of the incoming neutrons due to the fact that different magnetizations show different refractive indices for neutrons. The results are visible in the so called 'dark field image' of the specimen [35]. Local information on the inner domain wall density at different external magnetic fields applied can be obtained. In fact, as lower the domain wall density is, as bigger the average domain size is and then the macroscopic magnetization [9].

3.2.4 Local Magnetic Contrast

Local magnetic contrast is based on comparison of two images obtained by Kerr microscope which relies on Magneto-Optic Kerr-effect (MOKE) in order to see the state of magnetization on a surface of ferromagnetic material [36]. This method permits to see the displacement of wall domains when different value of magnetization is induced. Usually, this method is used together with integral measurements of fields and loss in all the sample to relate the contrast observed by microscope and the changes in magnetic properties. In this way, some relations can be found between domain wall displacement and magnetic degradation [37]. However, this method is surface sensitive, therefore if inner magnetic domain arrangement is different from the superficial one the results may not be reliable [38].

3.3 Summary

Direct and indirect methods to measure degradation of magnetic properties in ferromagnetic materials are presented in this chapter:

- Epstein frame and SST are standard measuring methods which allow high reproducibility rate. On the other hand, toroid and stator tests offer smaller reproducibility rate but they allow better representation of real condition of the electrical machine. These methods allow to measure the average rate of degradation in the whole strip.

- Direct methods are based on local measurements and observations and the approach is completely different from induction methods, except the fact that the search coils method is based on induction principle. Usually they are coupled with induction methods as reference to find a relation with average value on the strip.

- Search coils use induction approach applied at small region of specimen. However, inaccuracy due to the destructive approach can influence the results.

4 Cutting Techniques

Cutting of electrical steel causes changes in the structure of material on the cut edges. The main cutting techniques used in building of electrical machine are punching and laser cutting. Moreover guillotine, water jet cutting and wire electrical discharge machine are often used in experiments to study the effects of cutting. In this chapter, these techniques are presented and the results from literature are reported. A brief introduction of annealing is made at the end of the chapter. All the experiment reported are made on electrical steel. The samples are provided from the same roll, to avoid that the difference between the samples which could be greater than the degradation itself [39].

4.1 Mechanical Cutting

Mechanical cutting uses shear stress until shear strength of material is reached to cut the sheet. This process produces plastic strains and mechanical stress inside the material and affects the grains and the material structure as it is shown in Figure 6.

Punching and guillotine are examples of mechanical cutting, the first is used during building of electrical machines while the second is often used to produce samples for the Epstein frame during evaluation of specific loss of material. The cut between these two techniques is similar and it is expected that also the degradation on the material is equivalent.

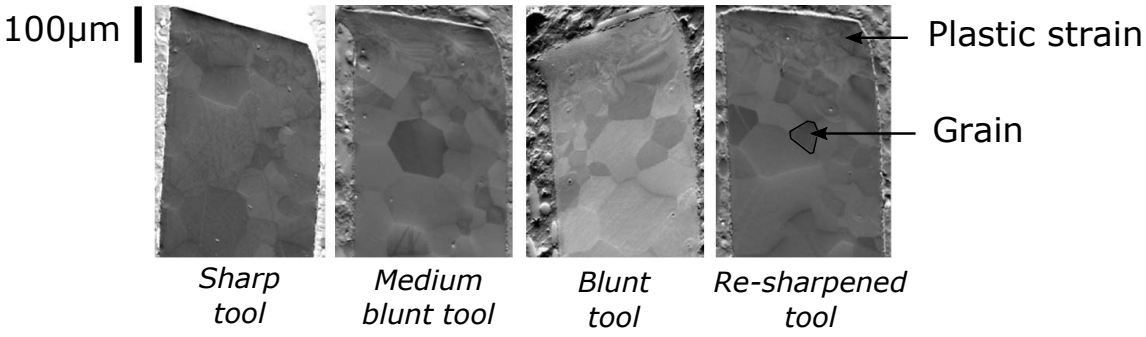

Figure 6: Cross sections of samples obtained by mechanical cutting with a sharp, medium blunt, blunt, and resharpened tool [41].

4.1.1 Punching

Punching is the most used cutting technique for production of electrical machines because of the manufacturing speed in case of big series production. Punching induces plastic deformation in the material modifying crystallographic texture of steel and degrading magnetic properties. Several parameters influence the degradation:

- Punch-die clearance influences shear stress and ductile fracture area [10], [40].
- Sharpness of the punching tool conditions the size of burr and deformed zone [10], [14].

- Thickness of the lamination and grain size are related to the propagation of stress inside material [9], [17]

It is not always possible to take into account all these factors, therefore, sometimes the reproducibility of the experiments is not guaranteed.

Permeability: Studies about punched samples obtained by means of Epstein frame evidence a drop of permeability after cutting process specially at low flux under knee of saturation in [42], [69]. Same results are obtained using SST [37], [44], [45]. Others studies by mean toroid test show similar degradation of permeability in [37], [46], [47].

Relation between rise of degradation and increasing size of grains as well as dropping of silicon content is reported in [48]. Results obtained by stator test in [49] suggest degradation of permeability and very high drop is quantified at 1,3 T and 50 Hz in [50].

Specific loss: according to [14], [51], [52] specific loss rises after cutting in particular at high flux density [42], in [16] it is evidenced that hysteresis loss changes more than eddy current loss, moreover in [48] increase in both excess and hysteresis component is found. Rise of losses is quantified by Epstein frame measurements from +10% [53], [69] until +20% by toroid tests in [37].

Depth of degradation: a depth of degradation of 10 mm is obtained by toroid test in [46] and [16]. Observations made by MOKE are reported in [37], where a depth of magnetically dead zone of 100-150 μm is observed at 1600 A/m (almost no magnetization) and 400 μm at 130 A/m in [9]. While, 750 μm of magnetically hardened zone at 120 A/m [48]. Dark-field image technique shows a degradation in the first 2,5 mm [45].

Coercive field: a rise of coercive field is observed in [37]. Increase of coercive field is probably related to the increase of pinning sites [36].

Annealing: reduction of punching effects after annealing are observed in [10], [37].

Hardness: Vickers measurements show hardness increasing in the first 1000 μm from cut edge [54] and almost 2000 μm in [55].

4.1.2 Guillotine Shear

Guillotine is composed by a static blade which supports the metal sheet and a moving blade. It works by first clamping the material with a ram then the moving blade down across the fixed blade to shear the material reaching the shear strength of the material.

Guillotine does not allow to cut a curved profile therefore is not used for building of machines but because of the lower cost of cutting it is preferred with respect to punching for preparation of strips used in Epstein frame. Moreover, cut edge and shear stress are similar to the ones obtained by punching and the studied effects are almost the same [17]. Therefore, many experiments analyse the guillotine cut in order to study the effects of punching.

The effects of cut are strongly linked to clearance, which is chosen between 2% and 10% of thickness of the sheet, and to the tool wear [41], [56], for instance see Figure 6 for the effects provoked by different sharpness of tool.

Permeability: In literature some experiments by means of Epstein frame show decrease of permeability [6], [53], [57], [58] in particular at low flux density [55], [69]. Also, the measurements by SST [59]–[61] and by means of ring toroid test have brought similar result [40].

Specific loss: Increase in losses is measured in [53] by 10%, in [56], [59] by 30%) and in [10] by 50%. In particular increase in hysteresis and excess loss components are observed, while classical loss remains almost constant [10], [43], [57].

Depth of degradation: Experiments with search coils show a depth of degradation between 5 mm [33], [40] and 10 mm [54], [59], [62]. results by SST, Epstein frame and toroid test show respectively 5 mm in [57], 10 mm in [63] and 15 mm in [10], [64]. Measurements by MOKE show a magnetically dead zone of 1000 μm at 120 A/m and 200 μm at 1450 A/m [10].

Grain size and silicon content: Correlation of degradation with bigger grain size is reported in [63], [65] and with higher silicon content in [23], [62].

Annealing and clearance: Restoring the effects of annealing after cutting are studied in [40], [64], [69] while in [56] reduction of degradation thanks to an optimal clearance is reported.

Hardness: According to the microhardness measurements in [56] a hardened zone of 0,5-1 mm is present on the cut edge, decreasing smoothly until 8 mm of depth. Increasing in hardness profile is observed on the first 400 μm in [40] and 1600 μm in [55]. Measurements for different clearances are taken in [56].

4.2 Laser Cutting

Laser cutting uses an energy emission device to focus a highly-concentrated stream of photons onto a small area to melt the metal and then blow molten material from the cutting area. Laser are typically computer-controlled and can make highly accurate cuts. It is slower than punching therefore, it is often used to build prototypes or for small-lot production [40], [53].

Neither shearing stress, nor burr are produced during cutting, nevertheless the high gradient of temperature generated to reach melting point of metal provokes thermal stress in relation with maximum temperature during the cut. Thermal stresses implicate micro-structural changes which affect the magnetic properties of steel.

Two main laser typology for cutting of metal sheets are CO_2 laser and Nd:YAG laser. Some parameters can influence the cut such as energy input, speed of cutting and volume flow of inert gas [33], [61]. Comparison between different experiments may be influenced by different parameters of machine and only qualitative observations can be done between results.

4.2.1 CO_2 Laser

CO_2 laser is a gas-laser that uses carbon dioxide (CO_2) as medium for the light beam, it is a relatively efficient laser with a good beam quality, therefore, it is one of the most widely used laser type.

Permeability: Measurements by Epstein frame with strips cut by CO_2 laser show very high degradation at low flux density if compared to mechanical cutting while, almost no effects appear at flux density higher than 1,5 T [40], [55], [66], same results are found with SST [67] and toroid test [37].

Specific loss: After cutting, increase in losses is observed for hysteresis component in [57] and also for excess component in [10]. A comparison between mechanical and laser cutting by means of Epstein frame and toroid test shows higher loss for laser [10], [37], [57] while, for high flux density losses in mechanical cut samples are higher than ones in laser cut [60].

Depth of degradation: Measurements by means of search coils presented in [33] show a depth of degradation of 2 mm at low flux density in some of the samples. MOKE observations in [37] shows a depth of degradation of 300 μm at low H-field (130 A/m) and no effect at high flux while, in [10] depth of degradation of 1000 μm at 120 A/m and 600 μm at 1450 A/m is observed.

Hardness: Vickers measurements show that no increase in hardness is generated by laser cutting [40], [54], [55]. Only for low-alloyed silicon steels a heat affected zone of 20-37 μm constituted by very fine microstructure is observed. For high-alloyed silicon steels material textures are similar to the one of base metal [68].

4.2.2 Nd:YAG Laser

Nd:YAG is a solid state laser where diode supplies a light beam that is amplified by a crystal of neodymium-doped yttrium aluminium garnet (Nd:YAG). It has a wavelength of 1,064 μm which is optimally suited for metals. This type of lasers includes relatively expensive pump diodes that have to be changed each 10.000 laser hours therefore, maintenance is quite expensive. Results obtained from samples cut by Nd:YAG laser are reported from the literature.

Permeability: Drop of permeability at low flux is measured by Epstein frame in [6] while at high flux there are negligible effects [69], similar results obtained by SST are presented in [45], [61]. Experiments by search coils show no effects at 1,5 T [40] while, very high degradation is found by mean toroid test in [54].

Specific loss: Increase of loss is revealed in [69].

Depth of degradation: Observations by DFI show a degradation of all the 10 mm width strip only from one cut edge in [9]. This result seems in contrast with previous experiments.

4.3 Wire Electrical Discharge Machining

Cutting by wire electrical discharge machining (WEDM) is due to the erosion that occurs when a spark forms between the cutting wire and raw material. As well as laser, it does not lead shearing deformation at the cutting edges and no burrs are formed. The spark can induce thermal stresses in the sheet but are almost negligible [64]. It is a very good method to avoid degradation on cutting edges but low cutting speed makes this method suitable only for trial manufacture or experiments [10], [40].

Permeability and loss: This technique produce small permeability degradation and negligible increasing in losses [48], because of that, it is assumed in some papers that the cut edge obtained by WEDM is not damaged [17], [37], [70].

Depth of degradation: Observations by MOKE shows very narrow degraded area of 200 μm at 120 A/m and 100 μm at 1450 A/m [10].

If WEDM is compared with mechanical, laser and water jet cutting, it results that WEDM give the smallest degradation at 1.5 T and the best results of power loss behind only water jet cutting. However, small degradation can be seen if compared with annealed samples [40], [48], [55].

4.4 Water Jet Cutting

Water jet cutting technology uses high pressure water with abrasive particles. The cut is obtained by erosion and it leads to a good cut quality on the top side but burrs on the other side. It does not cause shearing stress and the cooling effect of water avoid thermal stresses [71]. However, the low cutting speed leads to use water jet only for prototype and is recommended in particular for electrical machines with low and medium flux density range [72].

Among the other cutting techniques, the water jet is the one that produce least increase in specific loss [55], and in some studies is compared with annealed samples [72]. In [71] the samples cut by water jet shows the higher permeability if compared with specimens cut by other methods.

4.5 Stress Relief Annealing

Stress relief annealing can be introduced after cutting processes to restore steel properties and to eliminate the additional stresses [63]. The best effects result in mechanical and laser cutting but also WEDM and water jet take advantage from annealing [55]. In some cases, like synchronous reluctance machines where magnetic path on the rotor is obtained with several segments and many cut edges are present annealing is worth especially in high efficiency machines [7]. However, for most of the machines comparisons between annealing costs and machine performance improvements have to be evaluated. In fact, heat treatment should be kept for a duration between few minutes and one hour plus cooling time, increasing time and costs of production [7].

4.6 Summary

In this chapter the effects of different cutting techniques on magnetic properties are reported from literature.

Permeability: Decrease in permeability is more present at low flux densities in particular for laser while, mechanical cutting influences material also at high flux density.

Loss: increase of specific losses is in accordance with permeability decrease. Mainly hysteresis and excess components are influenced.

Depth of degradation: Indirect methods bring an average depth of degradation of 5 mm for mechanical cutting while, direct methods show degradation between 1 and 2 mm from the cut edge. For laser cutting a single experiment based on search coils reports 2 mm of depth of degradation against 1 mm obtained by MOKE.

Water jet cutting, WEDM or post cutting annealing allow to produce specimens with negligible degradation due to cutting with expense of higher cost and time.

5 Experimental Setup

In this chapter the configuration of the measuring system is reported. In the first section measuring devices used are briefly described. In the second section strips and configurations of strips used in the experiment are presented.

5.1 Measuring System

This section describes the devices used for measurements: custom made Epstein frame, data acquisition device, differential probe, shunt resistor, power supply, feedback control and variable resistor.

5.1.1 Customized Epstein Frame

Epstein frame used for the experiment had been built in the laboratory and is fitted to measure samples of 600 mm length and 60 mm width, that is almost the double of standard size according IEC [24]. Using wider strips allows a more homogeneous distribution of flux inside the magnetic path, moreover, 60 mm wide samples are less influenced by the edge effects with respect to samples of 30 mm wide.

Primary and secondary windings are formed by four coils with 170 turns each wound around the supports for the samples, see Figure 7. The specimens are inserted inside the coils forming a square. Four weights can be positioned above the extremities of the samples to fix them and guarantee a small air gap between the strips.

As suggested in standard IEC [24] a mutual inductor with variable number of turns is built to compensate the air flux within the secondary winding, otherwise this flux would contribute to the voltage at the secondary. The calibration of number of turns in the mutual inductor is obtained bringing the voltage of the secondary to zero during a measurement without samples.

The magnetic path L_m^* used to calculate the field strength is obtained with a simple proportion:

$$L_m^* = L_{ms} \frac{L^* - W^*}{L_s - W_s} \tag{12}$$

where L_{ms} is the standard length of magnetic path, L^* and W^* are length and width of the samples while L_s and W_s are length and width of the standard samples.

5.1.2 Data Acquisition Device

The measurements of voltage and current are obtained by a data acquisition device (DAQ) of National Instrument (NI USB-6251). The device has a sample rate of 1.25×10^6 samples per second allowing to collect 501 samples per cycle at 600 Hz.

Two auxiliary devices are used to connect the DAQ to the rest of the system: a differential probe (Tektronix P5200A) and a shunt resistor.

The differential probe has attenuation of 50× and is used to maintain the voltage measurement within the range of the DAQ. It is connected in parallel with the

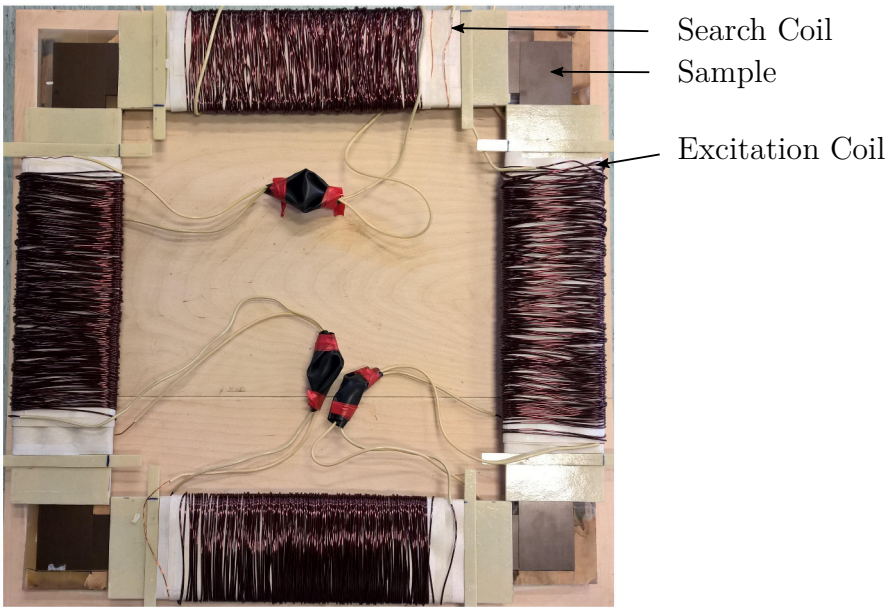

Figure 7: Epstein Frame used for the experiment.

terminals of secondary winding. The shunt resistor is rated 300 mA/86,728 mV and is used to convert the current value in a voltage signal for the DAQ.

The sample rates used for the measurements are proportional to the frequency maintaining 501 samples per period within all the frequency range (from 5 Hz to 600 Hz).

5.1.3 Power Supply

The power supply (Elgar SW 5250A) is set to external input and is controlled by computer that uses a feedback control. Power supply is used in ac mode. The ac mode is preferred over ac/dc mode to reduce the direct component of current supplied maintaining the symmetry of hysteresis loops. The shortcoming of ac mode is higher presence of low order harmonics in the supplied voltage but with negligible amplitude.

Some problem with the noise generated by the power supply has been met when amplitude of voltage signal at the secondary was very low and almost at the same amplitude of the noise, this happens for low frequencies according to Equation 10 where voltage is proportional to the frequency. For this reason, lowest frequency is set to 5 Hz.

5.1.4 Feedback Control

The feedback control is implemented in Matlab. The main controller is constituted by two different proportional controllers. One checks the amplitude of the voltage signal of the secondary winding and the second checks the fundamental harmonic amplitude to fix the form factor. When both controllers reach an error<2%, iterations are interrupted. In saturated region the feedback control adjusts the voltage of the

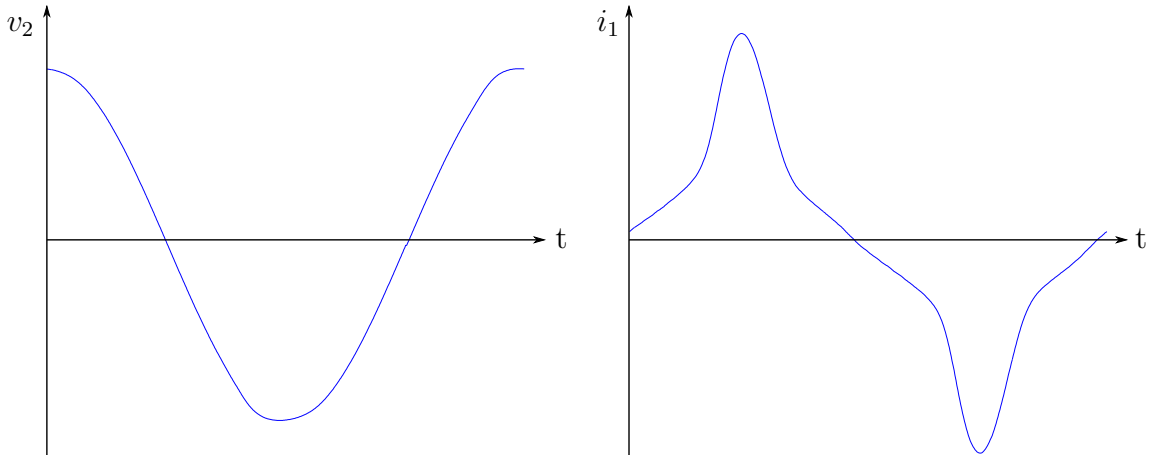

Figure 8: Voltage in the secondary and current in the primary of the Epstein frame after the iterations at 1,55 T and 50 Hz.

power supply obtaining a sharper current waveform. For example, during saturation at 1,55 T current supplied by generator assumes the shape in Figure 8.

Proportional control is fast outside saturated region but because of the offset error due to the absence of an integrator the control becomes slow to reach convergence at deep saturation. To avoid a slow convergence during measurements maximum flux density is set to 1,55 T.

5.1.5 Variable Resistor

At low frequency, when the counter-electromotive force induced in the primary of the Epstein frame is lower than few volts, the power supply is not able to manage the low voltage and the output of the power supply becomes very noisy. A variable resistor in series of primary winding is used to increase the voltage supplied at low frequency. Parasitic effects in the resistance are neglected.

5.2 Experimental procedure

In this section samples and methodology used in the experiment are presented.

5.2.1 Samples

Samples are obtained as sheets of fully processed non-oriented electrical steel, M270-50A according standard DIN EN 10106, with a thickness of 0,5 mm. M270-50A is an alloy of iron and silicon content of 3%, this material is commonly used in building of rotating electrical machine and the value of the thickness is typical in cores of medium size electrical machines.

The samples are constituted by rectangular strips of different width which are cut from the same roll by guillotine and laser cutting.

For the whole experiment following strips are prepared:

- 44 strips with a width from 10 mm to 60 mm and length of 600 mm cut by guillotine, see Table 1. These strips are joined in 6 different configurations to obtain a group of samples with a width of 60 mm, necessary for measurements by mean of customized Epstein frame. The Figure 10 in Chapter 6 shows all the configurations.

- 68 strips with a width from 5 mm to 60 mm are obtained by laser cutting, see Table 1. These strips were assembled in 12 different configurations to obtain group of samples with a width of 60 mm, Figure 18 in Chapter 6 shows some of the configurations.

Each configuration has a different number of cut edges, meaning a different density of damaged material (red area in Figure 10 and 18). The minimal width of 10 mm for mechanical cutting strips and 5 mm for laser cutting strips are chosen according to the depth of degradation reported in the literature, see Chapter 4. Configurations of strips are identified by the number of cut edges.

The strips are held together by means of tape to preserve a good magnetic path with smallest possible air gap between the strips. Moreover, some weights are positioned on the four corners of the Epstein frame above samples to reduce the air gap where samples overlie.

Table 1: All the strips used in the experiment.

Guillotine		**Laser**	
No.	Width (mm)	No.	Width (mm)
24	10	48	5
4	20	4	10
4	30	4	15
4	40	4	20
4	50	4	25
4	60	4	30
		4	35
		4	40
		4	45
		4	50
		4	60

5.2.2 Range of measurements

Measurements are performed for a range of frequency from 5 Hz to 600 Hz and a range of flux density from 0,05 to 1,55 T. All the steps are reported in Table 2.

Frequency lower than 5 Hz and flux density lower than 0,05 T are affected by high noise therefore, below these values measurements are not taken in consideration.

Table 2: Steps of flux density and frequency chosen for the measurements.

B (T)	0,05	0,1	0,15	0,2	0,3	0,4	0,5	0,6	0,7	0,8
	0,9	0,95	1	1,05	1,1	1,15	1,2	1,22	1,24	1,26
	1,28	1,3	1,32	1,34	1,36	1,38	1,4	1,45	1,5	1,55
f (Hz)	5	10	25	50	100	150	200	250		
	300	350	400	450	500	550	600			

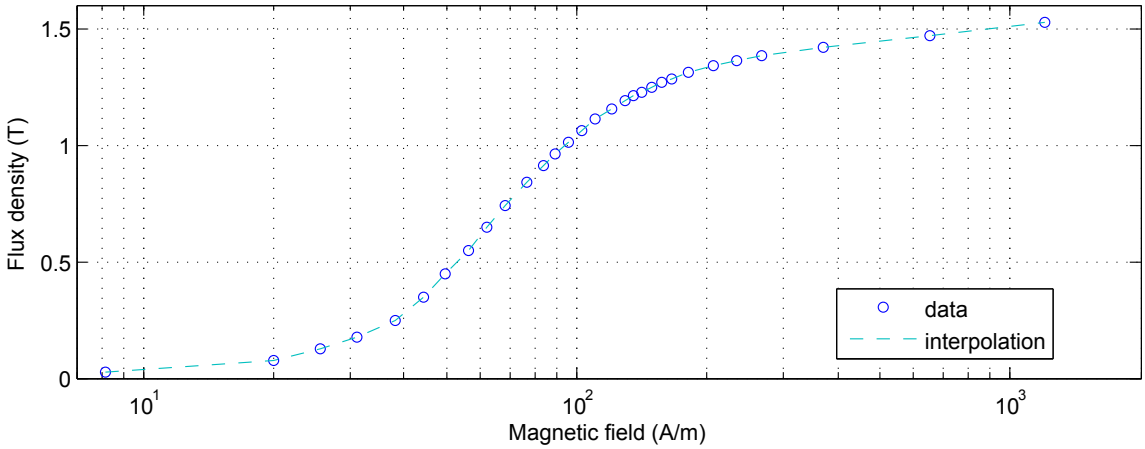

Figure 9: Example of the density of measurements for flux density, range from 0,05 to 1,55 T.

Flux density until 1,55 T guarantees good representation of magnetic behaviour also above the knee of saturation while for higher values the proportional feedback control has difficulty in convergence.

Flux density steps are denser between 1,2 to 1,4 T to obtain a better interpolation of BH curve along knee of saturation where strong non-linearity is present, see Figure 9.

5.2.3 Procedure

Strips are stuck together by tape forming four equal samples of 60×600×0,5 mm. Samples obtained are positioned in Epstein frame and four weights are put above samples on the four corners of Epstein frame.

A sinusoidal signal in the input of power supply is generated by the computer. Iterations controlled by feedback controller start and go on until the tolerance requested is reached.

To guarantee that measurements are taken at steady state, during each iteration Epstein frame is supplied by generator for several number of cycles. The transient is mainly due to induction of the coils. The end of transient of current at the primary and voltage at the secondary is checked by an external DAQ, in this way minimal number of cycles are supplied for each frequency saving time in particular at low frequencies. Number of cycles between 2 and 20 are used.

Instant values of voltage and current are collected by the DAQ, then B-field and H-field are calculated according Formulation 9 and 10.

The BH curves are obtained with a linear interpolation between all the couples of B maximum and H maximum. Then the absolute values of the complex permeability is calculated, see Equation 13.

The specific loss is obtained by Equation 11. The coefficients of hysteresis and classical loss of Jordan Model, see Equation 4, are obtained by surface fitting with the least squares method. Jordan Equation has been chosen because the simulation run successively needs as input those two loss coefficients.

5.3 Summary

This chapter presents how the experiment is managed, in particular:

- All the devices used during the measurements, their functions and characteristics.
- Range of flux density and frequency for the measurements are analysed and discussed .
- All the procedure followed during the measurement process is described step by step briefly.

Table 3: Configurations of strips for mechanical cutting and rate of damaged material.

Configuration	No. Strips	Cut Edges	Damaged material
1x60 mm	1	2	17 %
1x50 mm + 1x10 mm	2	4	34 %
1x40 mm + 2x10 mm	3	6	50 %
1x30 mm + 3x10 mm	4	8	67 %
1x20 mm + 4x10 mm	5	10	83 %
6x10 mm	6	12	100 %

6 Results of the Measurements

In this chapter method and results of the measurements are reported. In Section 6.1 and 6.2 results obtained from guillotine and laser cut samples will be presented, respectively.

6.1 Mechanical Cutting

In this section measurements obtained from mechanical cut samples are presented. First the strips configurations used then the results are reported. Starting with hysteresis loops, then BH curves, permeability and specific losses. A more complete report of data can be founded in Appendix A.

6.1.1 Configurations

The six configurations used are shown in Figure 10. The assumption followed is that degradation of the material spreads in the inner part of the strip in a constant way, see Figure 11, with a depth of penetration of 5 mm according to the literature, see Section 4.1.2. This means that all the damaged volume (red) is homogeneous and uniformly damaged. Under this assumption each configuration presents a different portion of damaged area proportional to the number of cut edges. The relation is reported in Table 3.

In the following each configuration will be identified in the legends by number of cut edges.

6.1.2 Hysteresis Loops

Hysteresis loops are obtained interpolating data of flux density as a function of field strength during a single period (interpolation among 501 samples). Loops show magnetic behaviour of material under induction in sinusoidal steady state. In particular remanence and coercive field are observed.

In Figure 12 (a) is shown hysteresis loop measured at 50 Hz and 1,55 T. It is possible to see the change of shape in the loop between the case with single strip (*2 cut edges*) that is almost not influenced by cutting and the configuration with 6 strips (*12 cut edges*) that is totally damaged.

Table 4: Rise of remanence and drop of coercive field after mechanical cutting.

1,55 T 50 Hz	**2 cut edges**	**6 cut edges**	**12 cut edges**
$\boldsymbol{B_r}$	0,903 (T)	-5,4 %	-15,3 %
$\boldsymbol{H_c}$	55,87 (A/m)	$+5,1$ %	$+10,6$ %

In Figure 12 (b) hysteresis loop is obtained at 250 Hz, where eddy current loss are the main component of loss and the loop is wider. In both cases knee of saturation is smoother in damaged material. Permeability is decreasing after cutting which is consistent with the literature.

Remanence B_r decreases by 15% after cutting, see Table 4. Coercive field H_c increases by 10%.

6.1.3 BH curves and permeability

The maximum values of flux density and field strength obtained for each hysteresis loop are interpolated to obtain the BH curves. BH curves are calculated for each frequency and configuration. The actual flux is not homogeneous over the whole sample due to the fact that the damaged and undamaged material has different permeabilities. Due to the nature of Epstein frame measurements the measured curves represent an average flux over the samples. Totally damaged configuration is the only configuration that presents uniform material, according the assumptions of

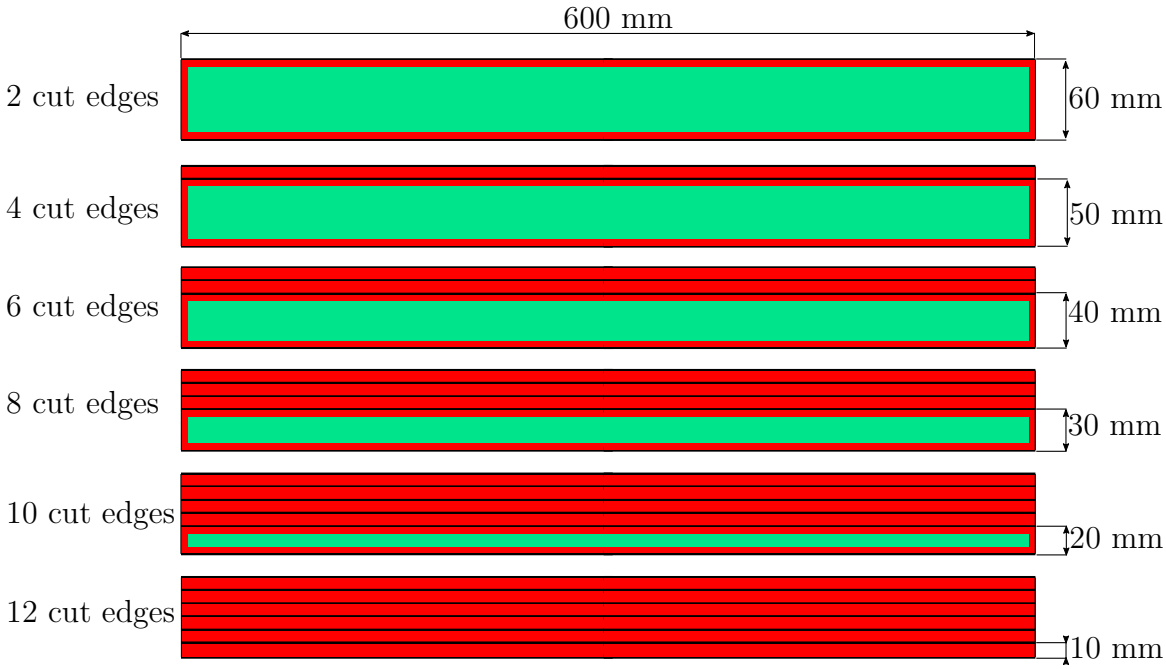

Figure 10: Strips configurations used for mechanical cutting. The green area is undamaged while red area is assumed damaged by cutting, with a depth of degradation of 5 mm.

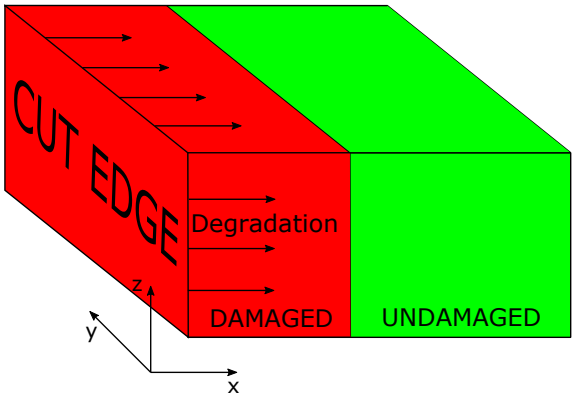

Figure 11: Assumption of uniform degradation along the cut edge, black arrows show spreading of degradation.

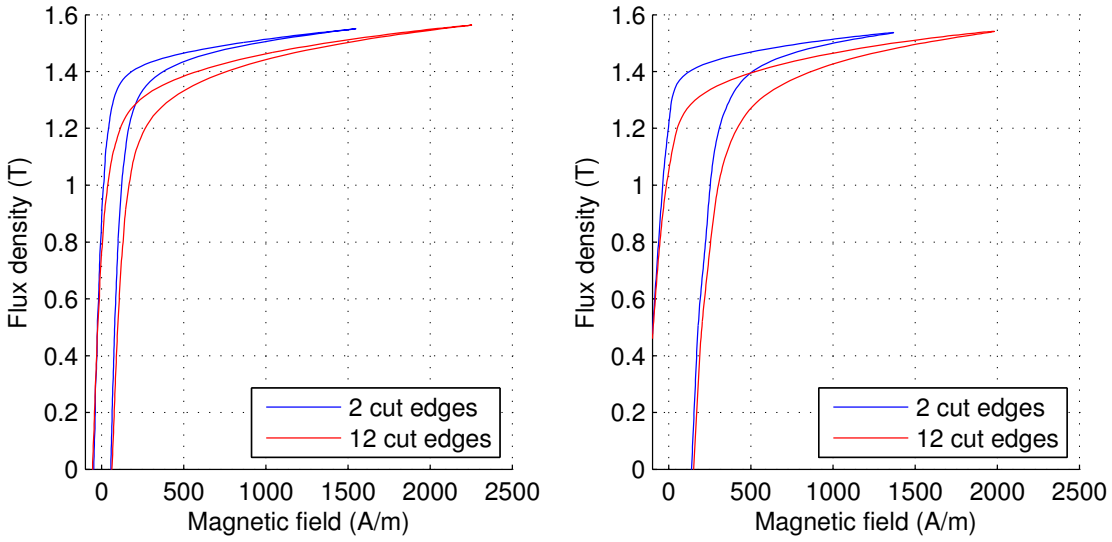

(a) 1,55 T 50 Hz

(b) 1,55 T 250 Hz

Figure 12: Hysteresis Loop at 50 Hz (a) and 250 Hz (b) at 1,55 T after mechanical cutting for *2 cut edges* and *12 cut edges* configuration.

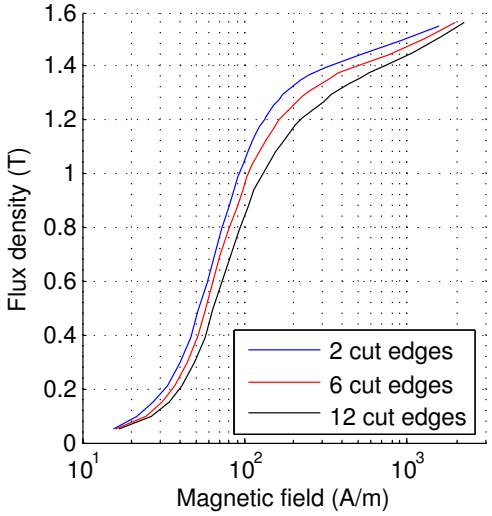

Figure 13: Comparison of BH curves at 50 Hz after mechanical cutting.

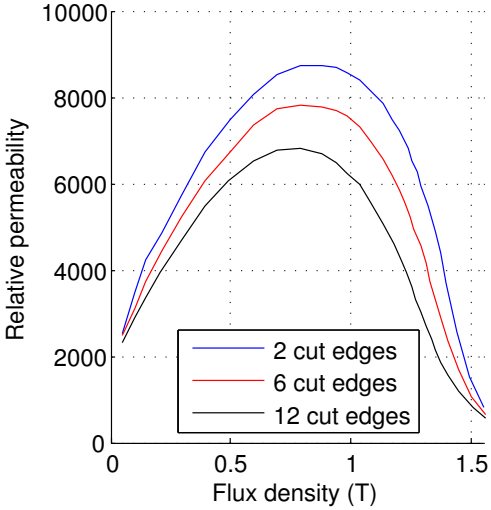

Figure 14: Drop of permeability at 50 Hz after mechanical cutting.

constant degradation along all the 5 mm of depth.

Three different configurations at 50 Hz are compared in Figure 13. A logarithmic scale is used to report better the behaviour at low magnetic field.

Permeability is calculated according the Equation 13:

$$\mu_{\mathrm{r}} = \frac{B_{\max}}{4\pi\mu_0 H_{\max}} \tag{13}$$

where $B_{\max}$ and $H_{\max}$ are the maximum values in the whole hysteresis loop, it means that in the case of delay of B with respect to H absolute value of complex permeability is considered. The permeability at 50 Hz as function of flux density is plotted in Figure 14. The decrease in permeability is maximum between 0,9 and 1,1 T in the region where electrical steel presents highest permeability.

Normalized values using *2 cut edges* configuration as reference are shown in Figure 15. The maximum relative decrease in permeability is at 1,4 T. According to the literature maximum drop of permeability should be at low flux density [43], [55]. However, measurements at 1,55 T show that permeability increases again after 1,4 T and overlapping between damaged and undamaged permeability curves is expected at higher saturation. Table 5 shows decrease in permeability after cutting at different values of flux density.

Decrease in permeability is obvious within all the frequency range, in particular at lower frequencies, while beyond 50 Hz the effect is weaker.

6.1.4 Specific Loss

Specific loss is calculated with Formulation 11 using data from measurements. As for permeability, also specific loss obtained is the average over loss from damaged and undamaged areas of the sample. Moreover, we assume that the distribution of

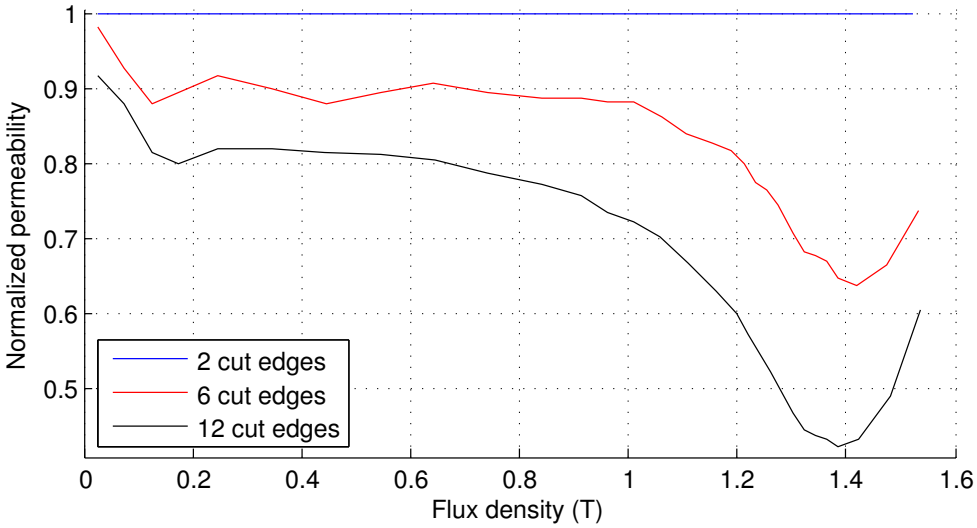

Figure 15: Relative permeability at 50 Hz normalized respect to *2 cut edges* configuration.

Table 5: Decrease in permeability after cutting at different values of flux density.

Drop of μ_r	**B**	**0,5 T**	**0,7 T**	**0,9 T**	**1,1 T**	**1,3 T**	**1,55 T**
2 cut edges	μ_r	7466	8593	8731	8156	6278	795
6 cut edges	(%)	-12,5	-9,9	-11,2	-15,8	-27,3	-21,6
12 cut edges	(%)	-19,0	-20,3	-23,3	-31,4	-52,1	-30,7

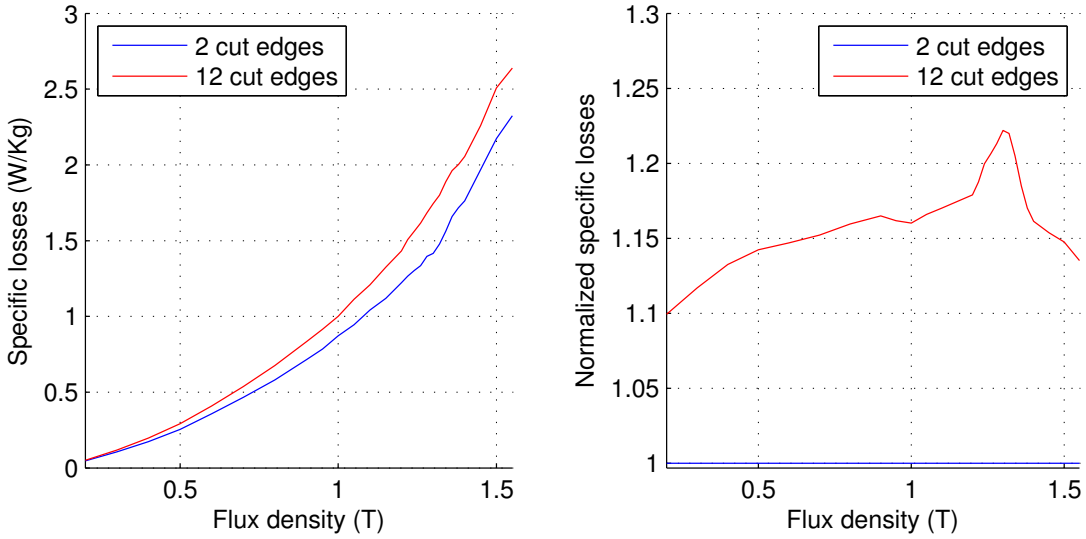

(a) (b)

Figure 16: Specific loss as function of flux density after mechanical cutting measured at 50 Hz (a) and normalized values (b).

flux is homogeneous, while in undamaged area flux density is higher because of the higher permeability with respect to the damaged area. Particular cases are the *2 cut edges* configuration where most of the material is undamaged and *12 cut edges* configuration where all the material is damaged.

The density ρ of material used in Equation 11 is obtained both from datasheet and weight measurements of specimens. The two values correspond within experimental error.

The loss at 50 Hz as function of flux density is plotted in Figure 16, where a comparison between different configurations is reported. Increase of specific loss at 50 Hz is more evident at high flux density, while the normalized value shows a peak close to knee of saturation at 1,3 T reaching +20% then it decreases until +15% at 1,5 T. The average rise along all the range of measurements is about 15%.

The loss at 1,5 T has been plotted as a function of frequency in Figure 17, a comparison between different configurations is reported. Table 10 shows rise of the losses after cutting at different values of flux density. Also in Figure 17 as for the precedent case, increase of specific loss is major at high values of frequency for both 1 T and 1,5 T cases, while the relative rising is higher at low frequency passing from about +15% at 50 Hz to +5% at 600 Hz in the case at 1,5 T induction. Inaccuracy of normalized values at low frequency (5-25 Hz) could be due to small absolute value of loss and therefore, small accuracy. According to Figure 17 (b) rise of specific loss at 1 T is more relevant (+15%) than the case at 1,5 T (+5%).

Table 6: Rise of loss after cutting as function of flux density.

Rise of Loss	**B**	**0,5 T**	**0,7 T**	**0,9 T**	**1,1 T**	**1,3 T**	**1,55 T**
2 cut edges	P (W)	$0,25$	$0,47$	$0,72$	$1,04$	$1,42$	$2,32$
6 cut edges	(%)	$+10,4$	$+6,8$	$+9,2$	$+8,0$	$+13,2$	$+7,3$
12 cut edges	(%)	$+14,4$	$+15,1$	$+16,6$	$+15,9$	$+23,2$	$+13,5$

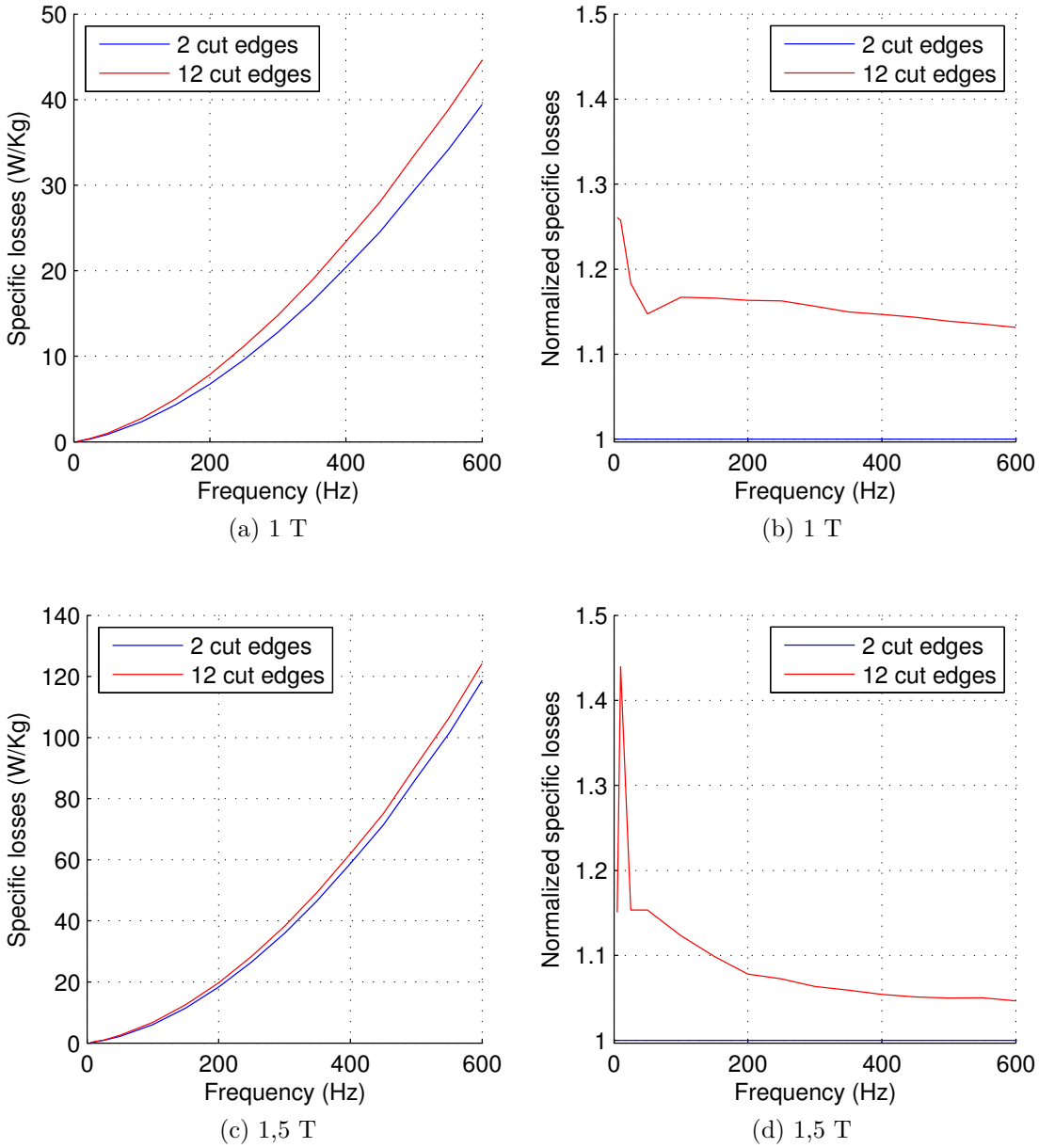

(a) 1 T (b) 1 T

(c) 1,5 T (d) 1,5 T

Figure 17: Specific losses as a function of frequency after mechanical cutting measured at 1 T (a,b) and 1,5 T (c,d) and normalized values.

6.2 Laser Cutting

In this section measurements obtained from laser cut samples are shown. First, the configurations used in the measurements for laser cutting are presented, then the results are reported starting with hysteresis loops, then BH curves, permeability and specific losses. Data from all the configurations are reported in Appendix B.

6.2.1 Configurations

The twelve configurations used for specimens cut by laser are shown in Figure 18. Same assumptions made for mechanical cutting in Section 6.1.1, with the difference that it is chosen a depth of penetration of 2,5 mm according to the literature [33]. Under this assumption each configuration presents a different portion of damaged area, proportional to the number of cut edges. The relation is reported in Table 7.

In the following each configuration will be identified in legends by number of cut edges.

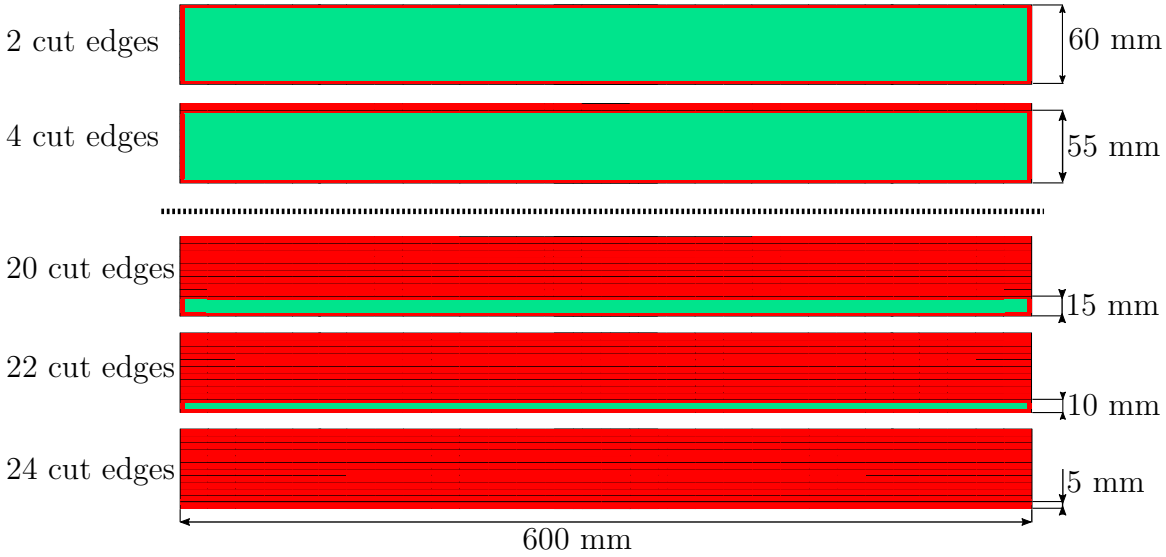

Figure 18: Configurations of strips obtained by laser cutting. Green area represents undamaged material while the red area represents the one damaged by cutting. The depth of degradation is assumed to be 2,5 mm.

6.2.2 Hysteresis Loops

In Figure 19 (a) hysteresis loop measured at 50 Hz and 1,55 T is shown. It is possible to see the change of shape in the loop between the case with single strip (*2 cut edges*) almost not affected by cutting and the configuration with 12 strips (*24 cut edges*) totally damaged.

In Figure 19 (b) hysteresis loop is obtained at 250 Hz, where eddy current loss is the main component of loss and the loop is wider. As expected permeability is decreasing after cutting. Remanence B_r decreases by -73% while coercive field H_c increases by 66%, see Table 8.

Table 7: Configurations of strips for laser cutting.

Configuration	No. Strips	Cut Edges	Damaged material
1x60 mm	1	2	8 %
1x55 mm + 1x5 mm	2	4	17 %
1x50 mm + 2x5 mm	3	6	25 %
1x45 mm + 3x5 mm	4	8	33 %
1x40 mm + 4x5 mm	5	10	41 %
1x35 mm + 5x5 mm	6	12	50 %
1x30 mm + 6x5 mm	7	14	58 %
1x25 mm + 7x5 mm	8	16	67 %
1x20 mm + 8x5 mm	9	18	75 %
1x15 mm + 9x5 mm	10	20	83 %
1x10 mm + 10x5 mm	11	22	92 %
12x5 mm	12	24	100 %

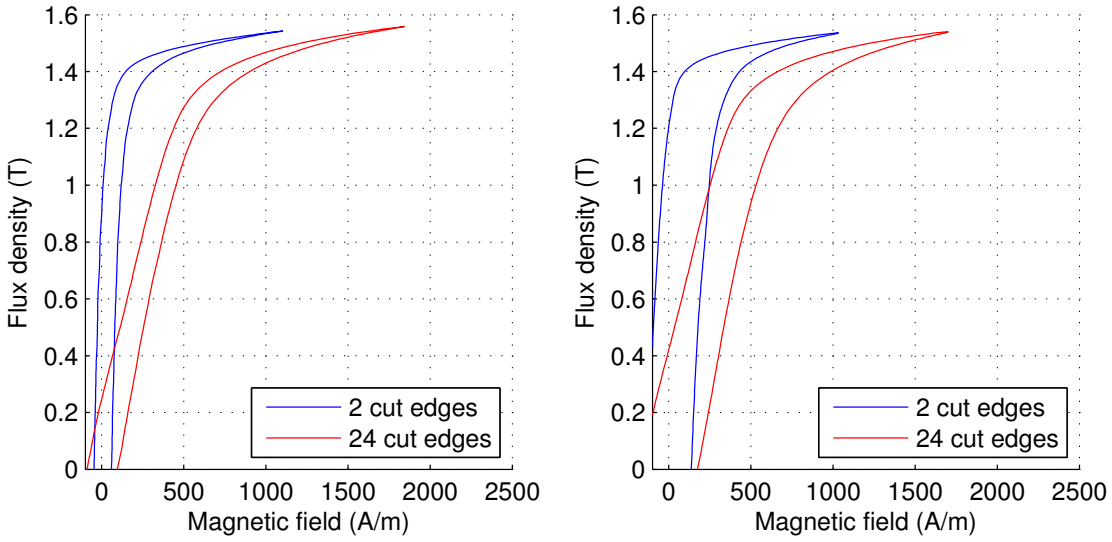

(a) 1,55 T 50 Hz (b) 1,55 T 250 Hz

Figure 19: Hysteresis Loop at 50 Hz (a) and 250 Hz (b) and 1,55 T after laser cutting for *2 cut edges* and *24 cut edges* configuration.

Table 8: Deviation of remanence and coercive field after laser cutting.

1,55 T 50 Hz	2 cut edges	6 cut edges	12 cut edges	24 cut edges
$\boldsymbol{B_r}$	0,894 (T)	-14,1 %	-39,8 %	-73,2 %
$\boldsymbol{H_c}$	59,36 (A/m)	+5, 7 %	+33, 4 %	+66, 6 %

6.2.3 BH curves and permeability

Four different BH curves at 50 Hz respectively for *2*, *6* ,*12* and *24 cut edges* are compared in Figure 20. A logarithmic scale is used to report in a better way the magnetization at low magnetic field.

Permeability is calculated according the Equation 13. The permeability at 50 Hz as function of flux density is plotted in Figure 21. A big decrease is observed over each configuration. In particular the *24 cut edges* configuration has a very flat curve with a value of relative permeability below 2000. All the four curves seem to converge at high flux density beyond 1,55 T.

In Figure 22 curves are normalized using the *2 cut edges* configuration as reference. The data shows that the maximum relative drop of permeability for *12 cut edges* is at 1,32 T and equal to -44,7%. With *24 cut edges* permeability is around -70% respect values of *2 cut edges* in all the flux range, but it rises to -40% at 1,55 T.

The different behaviour between *12 cut edges* and *24 cut edges* configurations is probably due to the strong inhomogeneity in *12 cut edges* configuration where half of the material is undamaged and half is damaged (see Figure 18), this causes a major concentration of flux in the undamaged area while in *24 cut edges* the distribution is more uniform since the material property is relatively homogeneous over the strips.

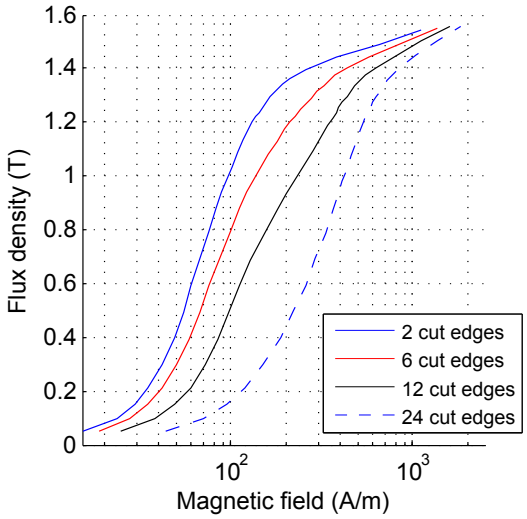

Figure 20: Comparison of BH curves at 50 Hz after laser cutting.

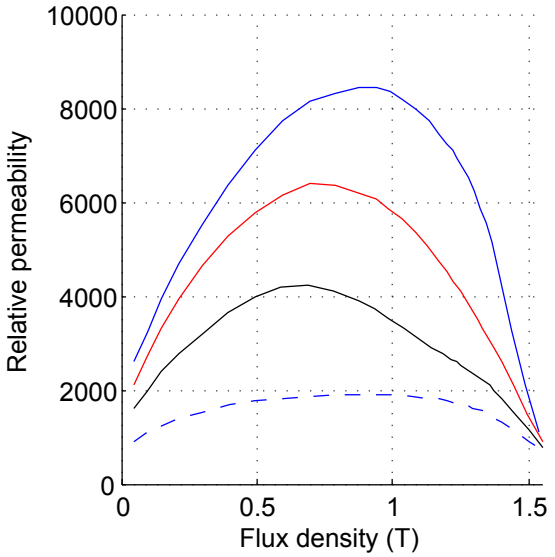

Figure 21: Drop of permeability at 50 Hz after laser cutting.

Table 9 shows decrease in permeability after cutting at different values of flux density, the maximum decrease is around 0,9 T while according to the literature [40], [55], [66] maximum drop of permeability should be at low flux density. However, measurements at 1,55 T show that permeability is increasing again after 1,4 T and overlapping of the two permeability curves is expected at higher saturation.

Results reported are at 50 Hz, and similar results are obtained also at the other frequencies.

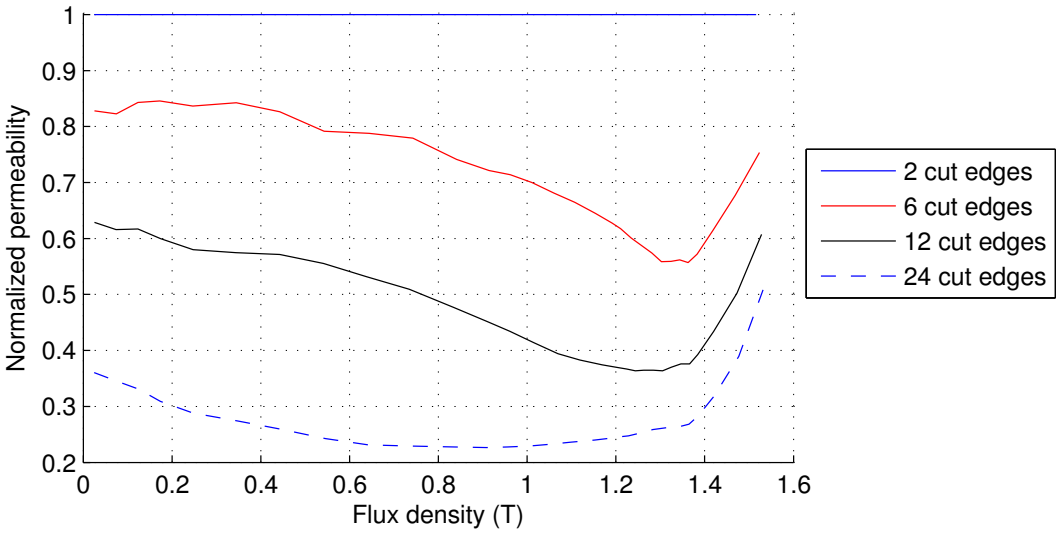

Figure 22: Relative permeability at 50 Hz normalized with respect to configuration with *2 cut edges*.

Table 9: Decrease in permeability after laser cutting at different values of flux density.

Drop of μ_r	**B**	**0,5 T**	**0,7 T**	**0,9 T**	**1,1 T**	**1,3 T**	**1,55 T**
2 cut edges	μ_r	7034	8198	8463	7990	6529	1113
6 cut edges	(%)	-19,0	-20,0	-27,6	-32,7	-43,5	-19,2
12 cut edges	(%)	-42,3	-51,5	-60,9	-66,9	-68,4	-39,8
24 cut edges	(%)	-74,7	-77,1	-77,4	-76,6	-74,4	-39,6

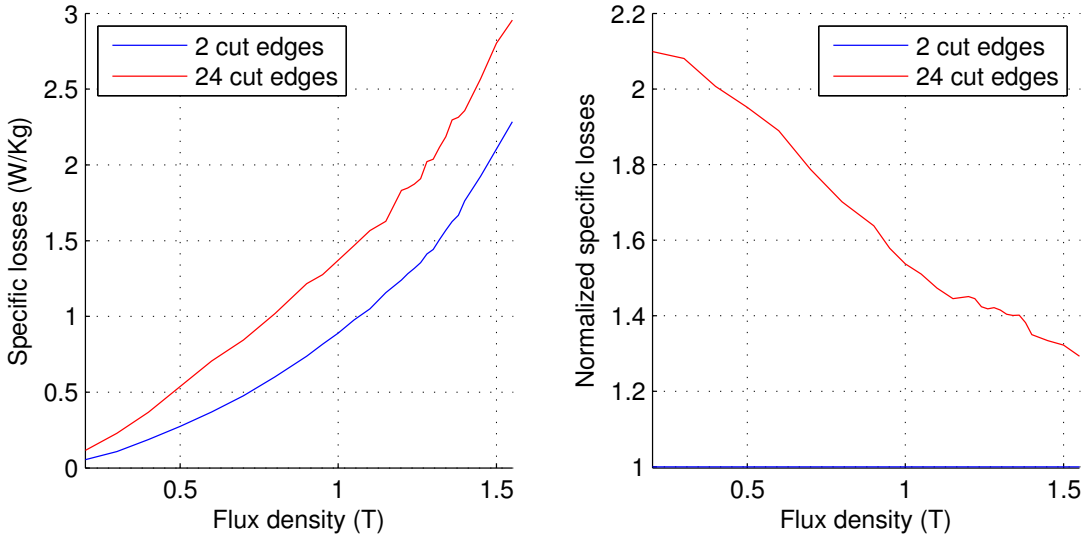

(a) (b)

Figure 23: Specific loss as a function of flux density after laser cutting measured at 50 Hz (a) and the normalized values (b).

Table 10: Increase in losses after cutting as a function of flux density.

Rise of Loss	**B**	**0,5 T**	**0,7 T**	**0,9 T**	**1,1 T**	**1,3 T**	**1,55 T**
2 cut edges	P (W)	$+0,27$	$+0,48$	$+0,74$	$+1,05$	$+1,44$	$+2,29$
6 cut edges	(%)	$+14,2$	$+20,3$	$+19,7$	$+18,5$	$+21,7$	$+18,9$
12 cut edges	(%)	$+45,3$	$+48,1$	$+48,2$	$+49,5$	$+45,4$	$+30,2$
24 cut edges	(%)	$+96,4$	$+77,2$	$+64,9$	$+49,1$	$+41,2$	$+29,3$

6.2.4 Specific Loss

Specific losses are calculated with Formulation 11 using the datas from measurements. The loss at 50 Hz is plotted as a function of flux density in Figure 23 and as a function of frequency in Figure 24. Comparison between different configurations is reported.

Normalized values show that losses after cutting are more than double at low flux density and about +30% at 1,5 T. We can assume that for higher flux density the effect of cutting on the losses will decrease until it disappear in accordance with literature [60]. Table 10 shows the increase in losses after cutting at different values of flux density.

Also in Figure 24 as for the precedent case, increase of specific loss is major at high values of frequency for both 1 T and 1,5 T cases, while the relative rising is higher at low frequency. This result confirms that dynamic losses, which are the main component at high frequency, are less influenced by cutting than hysteresis losses in agreement with [10].

Strange behaviour of normalized values at low frequency (5-25 Hz) could be due to small absolute values of losses and therefore, small accuracy.

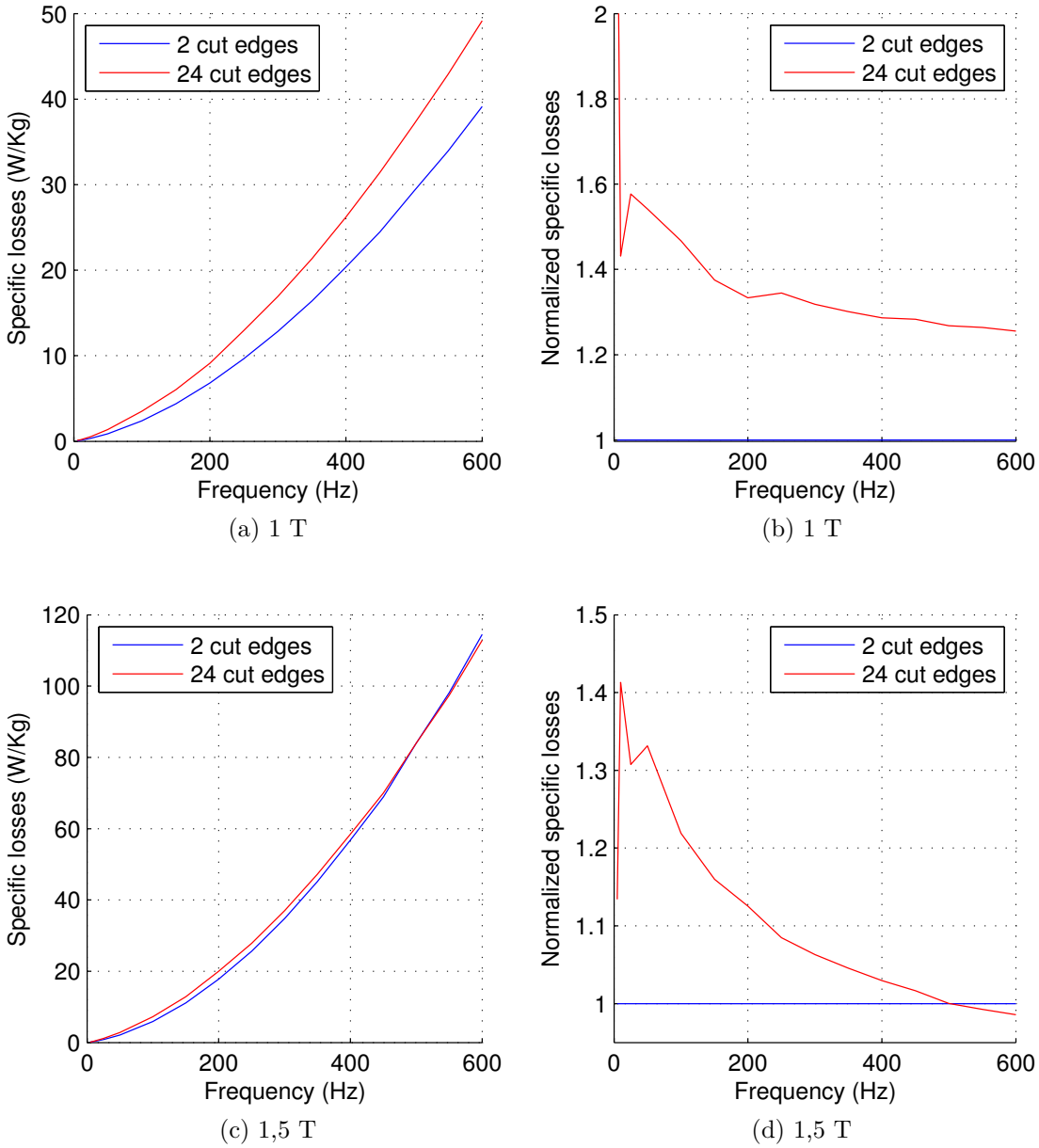

(a) 1 T (b) 1 T

(c) 1,5 T (d) 1,5 T

Figure 24: Specific losses as a function of frequency after laser cutting measured at 1 T (a,b) and 1,5 T (c,d) and normalized values.

6.3 Summary

In this chapter results of measurements are presented. The first section concerns the mechanical cutting while second section is about the laser cutting.

In both sections same scheme is followed:

- Brief presentation of the experiment, of the specimens used and the assumption made to support the data elaboration.
- Data from different configuration of strips are plotted to show deformation of hysteresis loop caused by cutting.
- Results from interpolation of hysteresis loops are reported to evidence decrease in permeability caused by cutting on specimens, absolute values and normalized ones are studied.
- Specific losses calculated as a function of flux density and frequency are presented.

7 Elaboration of the Measurements

In this chapter data obtained by measurements is analysed. First, a comparison between mechanical cutting and laser cutting is shown. Secondly, a curve fitting of the specific losses is presented and discussed. Finally, a finite element simulation on an induction motor and the results obtained are reported.

7.1 Comparison between Mechanical and Laser Cutting

Comparison between guillotine and laser cutting results obtained by measurements, in particular the effects on permeability and specific losses are evaluated.

7.1.1 Permeability

Permeability is calculated for all the different configurations of strips as seen in Chapter 6. The results obtained are plotted together to observe the change as a function of damaged material configuration. The degradation of material is proportional to the cut edges of the configuration (see Tables 3 and 7), therefore, a linear decrease of permeability between the samples could be found.

Normalized permeability at 50 Hz and for different values of flux density is plotted in Figure 25. The reference for the normalization is the *2 cut edges* configuration for mechanical cutting which represents well the undamaged material. The average width of strips corresponds to total width of sample divided by number of strips and is inversely proportional to the cut edges.

In Table 11 decrease in permeability at 50 Hz is compared between laser and mechanical cutting. Mechanical cutting damages 5 mm of material from the cut edge and halves the permeability in this area at 1,3 T while laser cutting reduces permeability of about 74% in the first 2,5 mm away the cut edge. At 1,55 T decrease is smaller, with -30% for mechanical and -40% for laser. In particular, we notice that at high flux density decrease is more similar between the two cutting techniques in agreement with [60].

The Figures 25 (a) and (b) are for flux densities at 1 and 1,2 T respectively. For these values of flux densities permeability decreases more quickly for laser than for mechanical cutting. The Figures 25 (c) and (d) report permeability for flux density at 1,4 and 1,5 T respectively. In this range the decrease in permeability caused by laser and guillotine appears almost equivalent. The decrease is quite proportional to the average width of strips, i.e. to the portion of damaged material.

Table 11: Comparison of permeability drop between mechanical (*12 cut edges*) and laser cutting (*24 cut edges*).

μ_r **at 50 Hz**		**0,5 T**	**0,7 T**	**0,9 T**	**1,1 T**	**1,3 T**	**1,55 T**
Mechanical Cutting	(%)	-19,0	-20,3	-23,3	-31,4	-52,1	-30,7
Laser Cutting	(%)	-74,7	-77,1	-77,4	-76,6	-74,4	-39,6

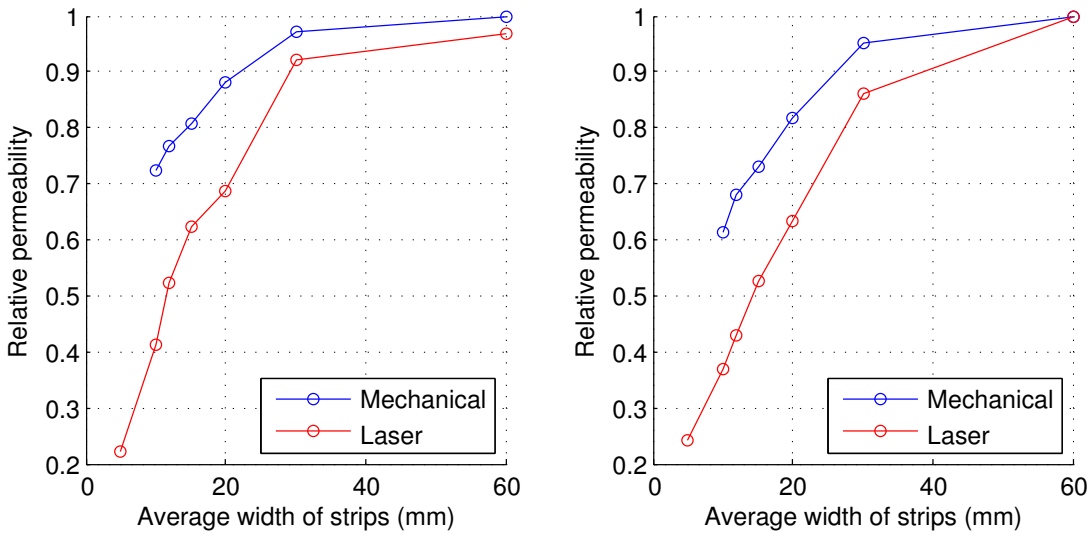

(a) 1 T 50 Hz

(b) 1,2 T 50 Hz

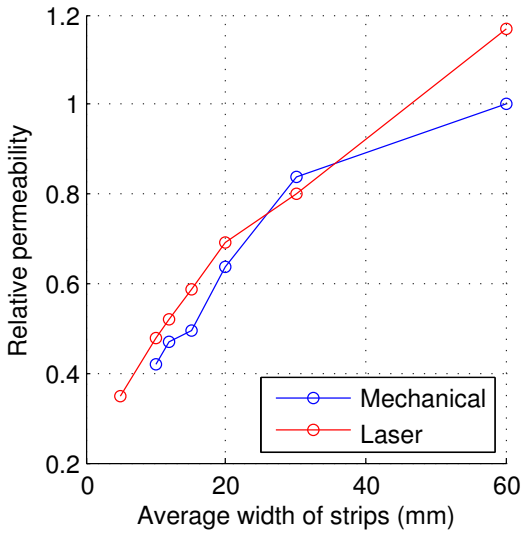

(c) 1,4 T 50 Hz

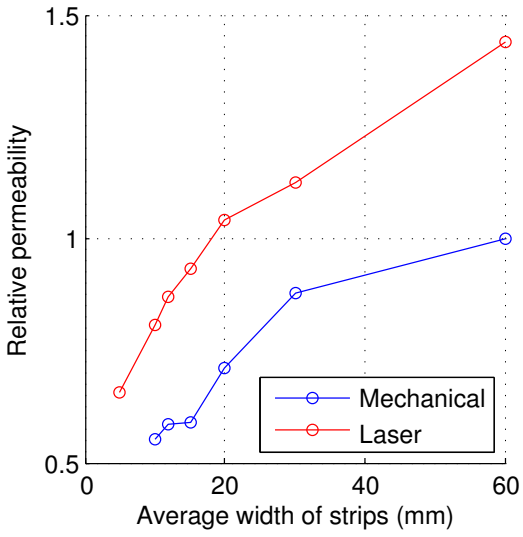

(d) 1,5 T 50 Hz

Figure 25: Normalized permeability at 50 Hz as a function of average width of strips for mechanical and laser cutting at different flux density 1 T (a) 1,2 T (b) 1,4 T (c) 1,5 T (d).

7.1.2 Specific Losses

In Figure 26 specific losses increase in relation with material degradation. Normalization of values with respect to the *2 cut edges* configuration describes the degradation of cutting better. The plots are referred to 50 Hz measurements. Losses increase almost proportional to the damaged area, but laser cutting causes steeper loss rising. This difference between the mechanical and the laser cutting is bigger at low flux densities (a),(b).

In Table 12 loss rise between undamaged (*2 cut edges*) and damaged material is reported. Laser and mechanical cutting are compared. The increase in losses provoked by mechanical cutting reaches +23% at 1,3 T and is smaller at 1,55 T with +13% whereas after laser cutting losses almost doubles at 0,5 T while, at 1,55 T an increase of 30% is measured.

Table 12: Comparison of increase in losses between mechanical and laser cutting at 50 Hz.

Specific Loss at 50 Hz		**0,5 T**	**0,7T**	**0,9 T**	**1,1 T**	**1,3 T**	**1,55 T**
Mechanical Cutting	(%)	+14, 4	+15, 1	+16, 6	+15, 9	+23, 2	+13, 5
Laser Cutting	(%)	+96, 4	+77, 2	+64, 9	+49, 1	+41, 2	+29, 3

7.2 Fitting of the Specific Losses

Specific losses are fitted with least squares method using Jordan Equation 4. In order to determine the loss coefficients surface fitting to the measured iron losses are realized for three cases where flux density and frequency was the chosen input variables. Data used for the interpolations are obtained respectively from:

1. *2 cut edges* mechanical cutting configuration which is assumed undamaged.
2. *12 cut edges* mechanical cutting configuration which is assumed total mechanically damaged material.
3. *24 cut edges* laser cutting configuration which is assumed total laser damaged material.

Surface fitting obtained for laser cutting is shown in Figure 27.

The hysteresis and dynamic loss coefficients obtained by fitting are reported in Table 13. It can be observed that the hysteresis coefficient k_{hys} increases more than the dynamic coefficient k_{dyn} in both mechanical (+23,3%) and laser cutting (+50,4%). This result is expected because the dynamic loss is mainly provoked by the induced eddy currents, which are not affected by the degradation how explained in [10]. Further, a decrease in k_{dyn} after laser cutting equal to -10,2% is calculated, this can be due to two main factors:

Table 13: Loss coefficients obtained from fitting of specific losses.

	2 Cut Edges (mechanical)	**12 Cut Edges (mechanical)**	**24 Cut Edges (laser)**
k_{hys}	1.733×10^{-2}	2.136×10^{-2}	2.607×10^{-2}
k_{dyn}	1.014×10^{-4}	1.069×10^{-4}	0.911×10^{-4}
k_{hys} **deviation**	0	+23,3 %	+50,4 %
k_{dyn} **deviation**	0	+5,4 %	-10,2 %

- The model used to describe the behaviour of specific loss is the Jordan Model, which has been developed for classical electrical steels and does not fit exactly the damaged material analysed as they have a bit different curve of losses.
- The width of the strips: 5 mm of width is equal to 10 times the thickness of the strip, in this condition the assumption made in [10], i.e. width $\gg$ thickness, is not satisfied.

7.3 Simulation by FCSMEK

In this section finite element simulation for a 37 kW induction machine is presented, characteristics of the motor are reported in Table 14. First, method used to describe the degradation of the material in the mesh is explained. Secondly, characteristics of simulations are reported. Finally, results are shown at the end of the chapter.

7.3.1 Layer Approach

To consider the influence of cutting a layer approach is followed. First, a layer is added to the original mesh of the machine along all the cut edges. The width of the layer is chosen equal to half width of the fully damaged strips used in the measurements. The layer has permeability and specific loss coefficients obtained from the measurements of damaged material. In this way, we can produce the effect of cutting process on the machine. Similar method with a multi-layer approach is used also in [39] and [74].

Two different meshes are created to apply the layer method. One for mechanical cutting with a layer of 5 mm and an other for laser cutting with a layer of 2,5 mm. The modified meshes are shown in Figure 28 where the damaged layer is purple while undamaged iron is grey. In addition to the layers data from *12 cut edges* configuration is used for mechanical case and from *24 cut edges* configuration which represent the wholly damaged materials. The permeability and the loss coefficients obtained from *2 cut edges* mechanical configuration are used in undamaged iron in all the cases.

In order to run the simulation required material parameters are conductivity, single-valued permeability as a function of flux density up to 2 T, hysteresis and dynamic loss coefficients. The conductivity is found on the material datasheet since

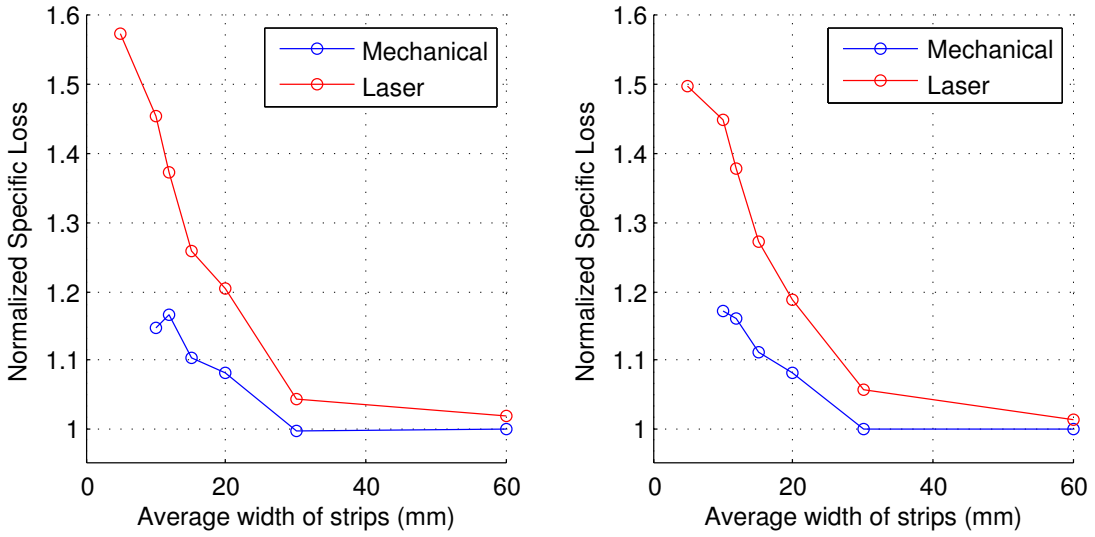

(a) 1 T 50 Hz

(b) 1,2 T 50 Hz

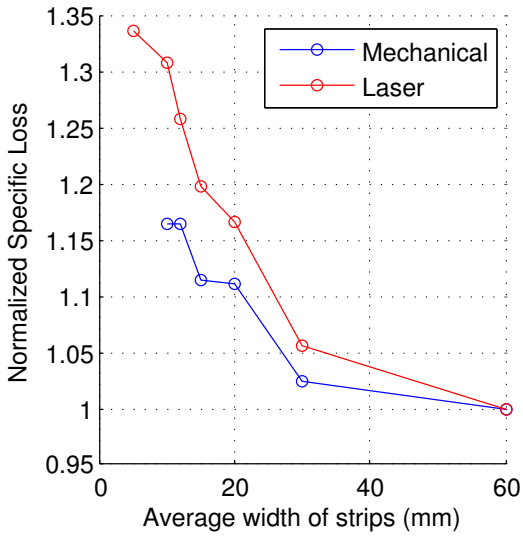

(c) 1,4 T 50 Hz

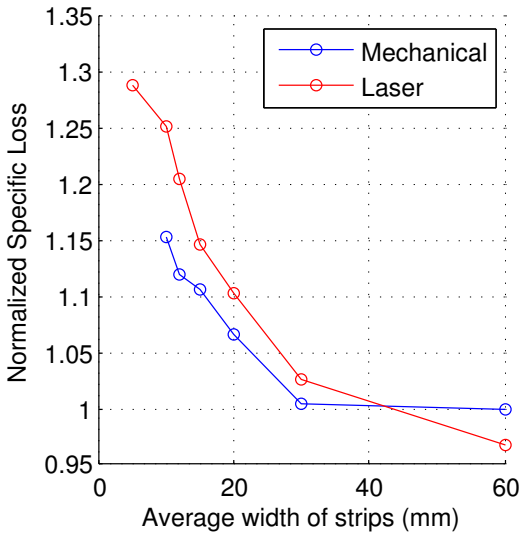

(d) 1,5 T 50 Hz

Figure 26: Specific losses at 50 Hz as a function of average width of strips for mechanical and laser cutting at different flux densities 1 T (a) 1,2 T (b) 1,4 T (c) 1,5 T (d).

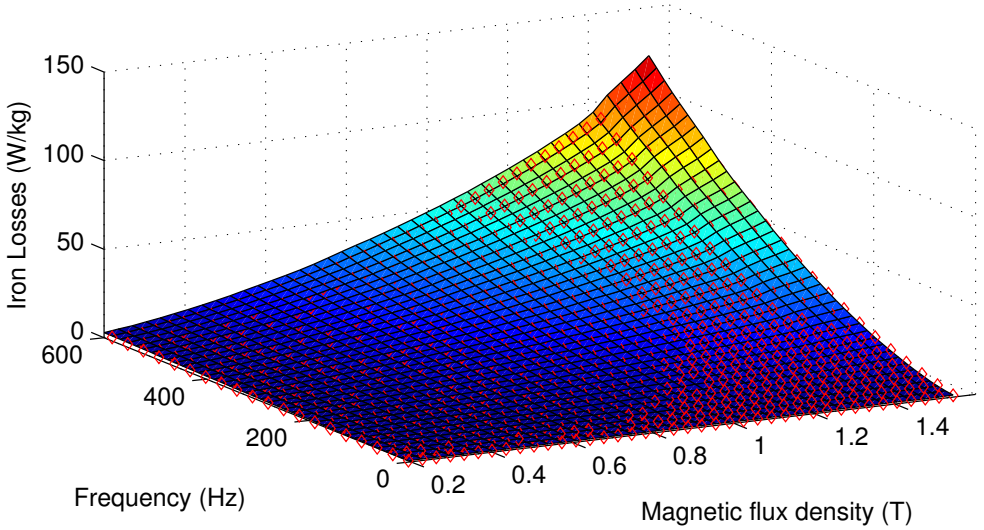

Figure 27: Surface fitting of the results from Jordan Model to the measured specific losses (red diamonds).

no degradation is assumed. Permeability is obtained from the measurements in the range of 0,05-1,55 T, then it is extrapolated to higher field using the model described in Equation 14:

$$\nu = \frac{1}{\mu_0 \mu_r} = \frac{a_1}{a_2}\left(1 + \left(\frac{B}{a_2}\right)^{a_3 - 1}\right) \tag{14}$$

where ν is the magnetic reluctivity while a_1, a_2 and a_3 are the coefficients obtained by the extrapolation. Using this model, single-valued BH curves of the damaged and the undamaged material overlap between 1,6 and 1,7 T. Beyond that point it is assumed that the effect of degradation is negligible and therefore, the same magnetization curve is used for flux density higher than 1,7 T. The loss coefficients used are obtained by surface fitting and they are previously reported in Table 13.

It is worth noticing that the difference between the two meshes in the teeth of the machine. While in mechanical case they are totally covered by the damaged layer, for laser cutting a path in the middle is present. This is caused as a result of choosing different layer width and it is expected to influence the flux distribution through the teeth of the machine as following: in the mechanical case the material is homogeneous and the flux in the teeth is uniform, while in the case of laser flux it is forced in the middle area which causes undamaged part to saturate earlier.

In total, three simulations were performed with three different meshes:

1. Undamaged machine: both iron and layer are characterised from undamaged material.

2. Machine obtained by mechanical cutting: inner iron is characterised from undamaged material while the layer is characterised from mechanically damaged material.

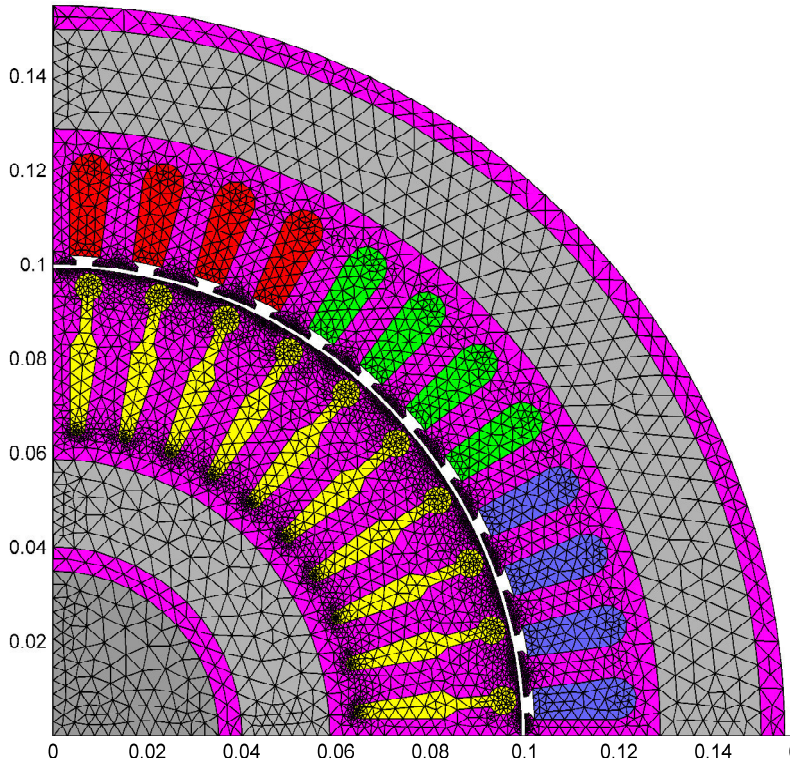

(a) Mechanical Cutting

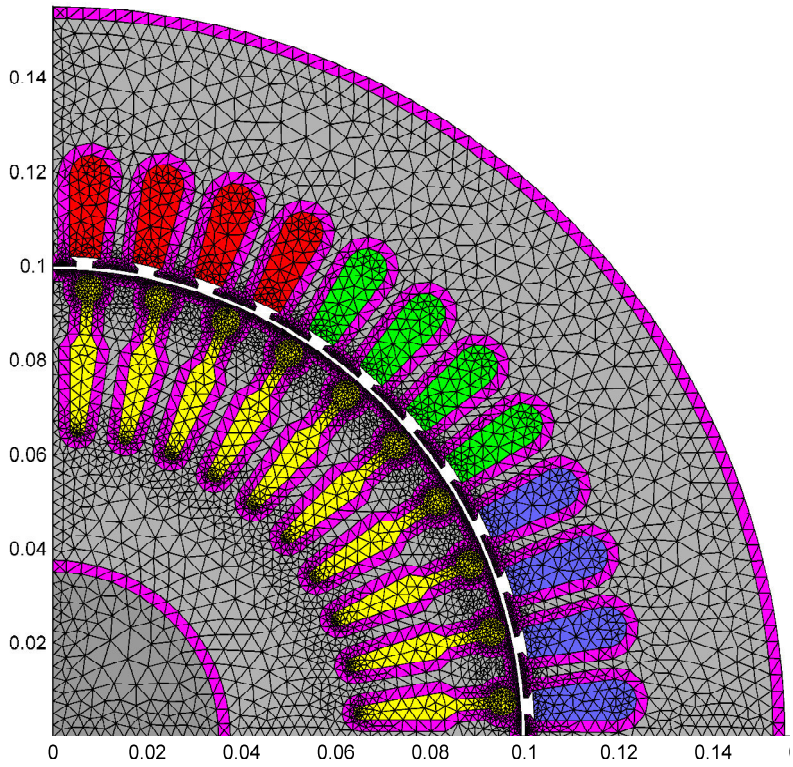

(b) Laser Cutting

Figure 28: Mesh modified with an additional layer of 5 mm for mechanical cutting (a) and 2,5 mm for laser cutting (b).

Table 14: Characteristics of the induction motor used in the simulations.

Shaft Power	37	kW
Voltage	400	V
Frequency	50	Hz
Connection	Star	
Number of pole pairs	2	
Stator outer diameter	310	mm
Stator inner diameter	200	mm
Air gap	0,8	mm
Number of stator slots	48	
Number of rotor slots	40	

3. Machine obtained by laser cutting: inner iron is characterised from undamaged material while the layer is characterised from the laser damaged material.

By means of these three simulations it is possible to compare the increase in losses caused by mechanical and laser cutting.

The simulations are executed by FCSMEK, a software based on finite element approach [75]. Each simulation is composed by two step, first a simulation in time-harmonic domain at 50 Hz is run to have initial conditions which is then used for performing a time-domain simulation to obtain the final results. Both voltage and shaft power are kept constant at 400 V and 33,5 kW in all the simulations while slip factor is modified. The value of shaft power is chosen to be close to the rated power.

7.3.2 Results from Simulations

The results of the three simulations (undamaged material, mechanical cutting and laser cutting) are reported in Table 15 where the mechanical cutting and the laser cutting are compared and the deviation with respect to the undamaged machine is presented.

From the results of the simulations some considerations are made as following:

- For mechanical cutting power factor decreases (-5%) and current in stator winding increases (+6%). This means that magnetization current is higher to supply same power shaft, because of the increase of reluctance in the teeth. This effect is not present in laser cutting because narrower damaged layer leaves an undamaged path along teeth which maintains relatively high magnetic permeance.

- Shaft power has a small deviation (-0,03% and +0,06%) due to the tolerance of the iterative method applied on slip factor to maintain the same power.

- Resistive losses in the stator increases due to increasing stator current.

Table 15: Results of the simulations for 37 kW induction machine.

	Unit	No Damage	Mech. Cut	Laser Cut	Mech. Cut (%)	Laser Cut (%)
Terminal voltage	V	400,00	400,00	400,00	0,00	0,00
Terminal current	A	56,36	59,73	56,87	+5,98	+0,90
Power factor		0,88	0,83	0,87	-5,43	-0,79
Slip	%	0,96	0,97	1,00	+1,35	+4,17
Rotational Speed	rpm	1485,60	1485,40	1485,00	-0,01	-0,04
Air-gap torque	Nm	215,37	215,39	215,60	+0,01	+0,11
Shaft power	kW	33,51	33,50	33,53	-0,03	+0,06
Air-gap flux density	T	0,87	0,86	0,87	-0,35	-0,12
Resistive loss stator	W	683,50	767,16	695,99	+12,24	+1,83
Resistive loss rotor	W	466,50	428,51	472,12	-8,14	+1,20
Total resistive loss	W	1150,00	1195,67	1168,11	+3,97	+1,57
Core loss in the stator	W	212,50	235,80	237,47	+10,96	+11,75
yoke	W	130,22	142,25	141,21	+9,24	+8,44
teeth	W	70,20	81,91	85,81	+16,68	+22,24
tooth tips	W	12,03	11,65	11,45	-3,16	-4,82
Core loss in the rotor	W	46,00	43,09	42,27	-6,33	-8,11
yoke	W	0,19	0,18	0,20	-5,26	+5,26
teeth	W	22,98	22,22	20,56	-3,31	-10,53
tooth tips	W	22,91	20,69	21,52	-9,69	-6,07
Total core loss	W	258,50	278,89	279,74	+7,89	+8,22
Total electromag. loss	W	1408,00	1474,56	1447,85	+4,73	+2,83

- Resistive losses in the rotor decreases only with mechanical cutting (-8%) mainly because lower permeability induces smaller current in the rotor cage with the same field strength.

- Stator core losses increase mainly because of higher loss coefficients at the damaged layer. In both cases similar increase is observed (+11%). Particularly, high increase in the teeth region takes attention (+17% and 22%). Although for the laser case damaged material is less amount due to the higher loss coefficients higher loss increase is observed, see Table 13.

- Core losses in the rotor decreases in the mechanical case (-6%) because of the lower flux distribution amplitude while in the laser cutting (-8%) it is decreased mainly due to lower dynamic loss coefficient compared to the undamaged case that effects eddy current losses induced in the tooth tips by angular speed of the rotor

- Total core losses are around 8% higher compared to losses in machine with undamaged material in both cases. The influence on total electromagnetic loss is +5% for the mechanical and +3% for the laser.

- Change in the efficiency is low, -0,2% for the mechanical cutting and -0,1% for the laser cutting.

Finally, distribution of the flux density in the machine calculated by finite elements is shown in Figure 29 for undamaged an laser damaged cases. Flux concentration in the undamaged part is clearly visible at the teeth region where low flux density distribution is present, whereas, teeth regions with high flux density distribution seem relatively unaffected.

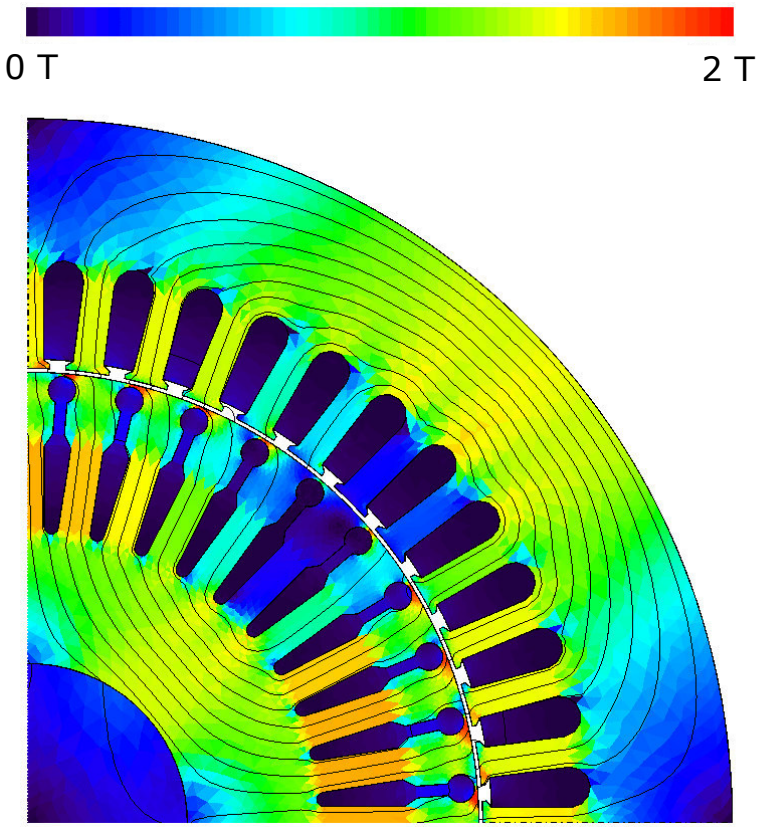

(a) Undamaged Machine

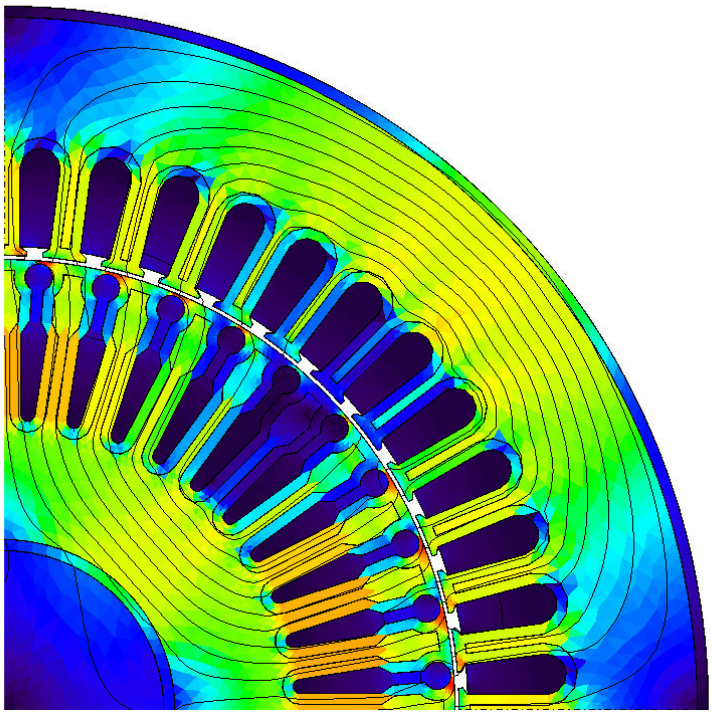

(b) Laser Damaged Machine

Figure 29: Flux distribution obtained by the simulations on the studied induction machine with undamaged material everywhere (a) and laser damaged material at the cut edges (b).

7.4 Summary

In this chapter further elaboration of the data obtained from the measurements and the simulations are presented:

- A comparison of the permeability decrease as function of degradation level is shown. From the plots a stronger effect of laser cutting compared with mechanical cutting is visible, in particular at low flux density, while at high flux the effect is similar.
- A comparison of the increase in iron losses as a function of degradation level is reported. Increase is bigger for the laser cutting into all the range of flux density but more pronounced at the low flux density.
- Results of loss coefficients fit is reported and discussed. Hysteresis component is strongly affected whereas small influence is observed for dynamic loss component for the damaged materials.
- Approach used for the simulation on a 37 kW induction machine is explained, then results obtained by the simulations are reported. Some conclusions about the simulation results are discussed at the end of the chapter.

8 Conclusions and Future Works

8.1 Conclusions

In this thesis's project the effects of guillotine and laser cutting on the non-oriented electrical steel M270-50A are measured by means of Epstein frame using strips of different size. The decrease in permeability and increase in losses after cutting are quantified.

The permeability after the guillotine cut reduces for all the studied range of frequency and flux density, in particular the maximum decrease is observed around the knee of saturation at 1,4 T. Laser cutting shows stronger influence along all the studied flux range, the effects are reduced only at flux densities higher than 1,4 T.

After the guillotine cut, specific losses increase of about 15% at 50 Hz, with a peak at 1,4 T. The increase is lower at high frequencies. Increase in losses is also present after the laser cutting, in that case is more evident at low flux density, and in particular at low frequency. The separation of losses obtained by interpolation shows that the hysteresis component is more influenced than the dynamic component for both guillotine and laser cutting. This result is in agreement with the theory about the strong dependence between hysteresis losses and pinning sites.

The finite elements simulation on a 37 kW induction machine shows that the iron losses of the studied machine increase by 8% after the effect of cutting is taken into account. Effects of laser and guillotine cutting results are similar, due to the effect caused by the wider damaged layer used in the guillotine cut case is compensated by the narrower damaged layer with higher loss coefficients in the laser case.

8.2 Critical Assessment

In this experiment homogeneous and constant degradation of steel is assumed. This is the simplest approach. However assuming a reduction of degradation leaving the cut edge with a linear or a quadratic behaviour is more realistic according the literature.

Depth of degradation is assumed according the literature. However, a study with narrower strips should be made to validate this assumption.

The reference for the undamaged material is the *2 cut edges* configuration, the cutting effect on this configuration is not negligible and the specimen should be annealed to reduce the degradation. Also water jet cut or WEDM can be used to obtain a less damaged sample.

Jordan Model used to fit the specific loss coefficients and calculated two components are adapted to represent the behaviour of electrical steel. However, degraded steel has a different behaviour with respect to typical electrical steel. Therefore, a modified loss model should be tested.

The length of magnetic path L_m of the customized Epstein frame is evaluated assuming the same path shape of standard Epstein frame. However, the strips do not maintain the same rate length/width causing a small error in the field strength.

8.3 Improvements and Future Works

The experiments are made by means of a customized Epstein frame. The use of standard Epstein frame should improve reproducibility of the experiments.

Increasing the measured maximum flux density beyond 1,55 T would increase the information in saturated material and would improve the accuracy of the further simulation.

Measurements for lower frequencies below 5 Hz would reduce the error on the hysteresis coefficients, which should be calculated at quasi-static state.

Simulation of smaller machines, used for example in light electric vehicle where the efficiency is still important, should show higher effects due to the bigger rate between damaged and undamaged material.

Minor loops and rotational fields are not considered in this work, therefore, a future work could deal with the effects of cutting on these fields.

Also other type of electrical steels such as grain oriented, permalloys, amorphous materials etc. could be measured to observe if the effects of cutting change in different materials.

References

[1] "Commission Regulation (EU) No 640/2009", *Official Journal of the European Union*, July 2009.

[2] "Commission Regulation (EU) No 4/2014", *Official Journal of the European Union*, July 2014.

[3] S. Steentjes, M. LeBmann, K. Hameyer, "Advanced iron-loss calculation as a basis for efficiency improvement of electrical machines in automotive application ", *Electrical Systems for Aircraft, Railway and Ship Propulsion (ESARS)*, Oct. 2012.

[4] M.J. Hofmann, H. Herzog, "Modelling Magnetic Power Losses in Electrical Steel Sheets in Respect of Arbitrary Alternating Induction Waveforms: Theoretical Considerations and Model Synthesis", *IEEE Transaction on Magnetics*, Vol. 51, No. 2, 2015.

[5] A. Schoppa, J. Schneider, J.O. Roth, "Influence of the cutting process on the magnetic properties of non-oriented electrical steels",*Journal of Magnetism and Magnetic Materials*, Vol. 215-216, pp. 100-102, 2000.

[6] R. Siebert, R. Baumann, E. Beyer, "Laser Manufacturing of Electrical Machine", *Electric Drives Production Conference (EDPC), 2014 4th International*, pp. 1-5, Sept. 2014.

[7] C. Liu, B. Chang, K. Hung, S. Lin, "Cutting and Punching Impacts on Laminated Electromagnetic Steels to the Designs and Operations of Synchronous Reluctance Motors", *IEEE Transactions on Industry Applications*, Vol. 51, No. 4, July 2014.

[8] Jürgen Reinert, Ansgar Brockmeyer, Rik W. A. A. De Doncker, "Calculation of Losses in Ferro and Ferromagnetic Materials Based on the Modified Steinmetz Equation", *IEEE Transaction on Industry Applications*, Vol. 37, No.4, 2001.

[9] R. Siebert, J. Schneider, E. Beyer, "Laser Cutting and Mechanical Cutting of Electrical Steels and its Effect on the Magnetic Properties", *IEEE Transaction on Magnetics*, Vol. 50, No.4, 2014.

[10] M. Hofmann, H. Naumoski, U. Herr, H. Herzog, "Magnetic Properties of Electrical Steel Sheets in Respect of Cutting: Micromagnetic Analysis and Macromagnetic Modeling", *IEEE Transaction on Magnetics*, Vol. 52, No.2, 2016.

[11] G. Bertotti, "General Properties of Power Losses in Soft Ferromagnetic Materials", IEEE Transactions on Magnetics, Vol. 24, 1988.

[12] G. Bertotti, “Comparison of Iron Loss Models for Electrical Machines With Different Frequency Domain and Time Domain Methods for Excess Loss Prediction", *IEEE Transactions on Magnetics*, Vol. 51, 2015.

[13] E. Barbisio, F. Fiorillo, C. Ragusa, “Predicting Loss in Magnetic Steels Under Arbitrary Induction Waveform and With Minor Hysteresis Loops", *IEEE Transactions on Magnetics*, Vol. 40, No. 4, July, 2004.

[14] A.C. Smith, K. Edey, “Influence of Manufacturing Processes on Iron Losses", *Electrical Machines and Drives*, 1995.

[15] P. Goes, E.Hoferlin, M. De Wulf, “Calculating Iron Losses Taking into Account Effects of Manufacturing Processes", *Excerpt from the Proceedings of the COMSOL Conference 2008 Hannover*, 2008.

[16] A. Boglietti, A. Cavagnino, L. Ferraris, M. Lazzari, “The Annealing Influence onto the Magnetic and Energetic Properties in Soft Magnetic Material after Punching Process", *Electric Machines and Drives Conference, 2003. IEMDC'03. IEEE International*, Vol. 1, June 2003.

[17] L. Vandenbossche, S. Jacobs, F. Henrotte, K. Hameyer, “Impact of cut edges on magnetization curves and iron losses in e-machines for automotive traction", *World Electric Vehicle Journal*, Vol. 4, 2010.

[18] C. Steinmetz, “On the law of hysteresis", *Proceedings of the IEEE*, Vol. 72, No. 2, pp. 197-221, 1984.

[19] M. Reinlein, T. Hubert, A. Hoffmann, A. Kremser, “Optimization of analytical iron loss approaches for electrical machines", *Electric Drives Production Conference*, pp. 1-7, 2013.

[20] J. Li, T. Abdallah, C. Sullivan, “Improved calculation of core loss with nonsinusoidal waveforms", *Industry Applications Conference*, vol. 4, pp.2203-2210, 2001.

[21] G. Bertotti, “Physical interpretation of eddy current losses in ferromagnetic materials. Theoretical considerations", *Journal of Applied Physics*, Vol. 57, 1985.

[22] R. Rygal, A.J. Moses, N. Derebasi, J. Schneider, A. Schoppa, “Influence of cutting stress on magnetic field and flux density distribution in non-oriented electrical steels", *Journal of Magnetism and Magnetic Materials*, Vol. 215-216, pp.687-689, 2000

[23] A. Peksoz, S. Erdem, N. Derebasi, “Mathematical model for cutting effect on magnetic ?ux distribution near the cut edge of non-oriented electrical steels", *Computational Materials Science*, Vol. 43, 2008.

[24] “IEC 60404-2, Magnetic materials. Part 2: Methods of measurement of the magnetic properties of electrical steel sheet and strip by means of an Epstein frame", 1996.

[25] R.S. Albir, A.J. Moses, “Improved dc bridge method employed to measure local power loss in electrical steels and amorphous materials", *Journal of Magnetism and Magnetic Materials*, Vol. 83, pp. 553, 1990.

[26] J. Bajoreki, D. Gaworska, “Measurement of the losses of electrical steel sheet samples at high magnetic flux density", *Przegled Elektrotechniczny*, No. 6, pp. 125-127, 2012.

[27] C. Appino, F. Fiorillo,C. Ragusa, B. Xie, “Magnetic losses at high flux densities in non-oriented FeSi alloys", *Journal of Magnetism and Magnetic Materials*, pp. 2526-2529, 2008.

[28] “IEC 60404-10,Magnetic materials. Part 10: Methods of measurement of magnetic properties of magnetic sheet and strip at medium frequencies", 1988.

[29] T. Nakata, N.Takahashi, Y.Jawase, M.Nakano, M.Miura, J.D. Sievert, “Numerical analysis and experimental study of the error of magnetic field strength measurements with single sheet testers", *IEEE Transaction on Magnetics*, Vol. 22, 1986.

[30] Y. Zhang, “Magnetic core losses measurement instrumentations and a dynamic hysteresis loss model", *Electrical Power and Energy Conference*, pp. 1-5, 2009.

[31] A. Krings, J. Soulard, “Experimental Characterization of Magnetic Materials for Electrical Machine Applications, Electrical Machines Design", *Control and Diagnosis (WEMDCD)*, pp. 85-89, 2015.

[32] G. Crevecoeur, P. Sergeant, L. Dupré, L. Vandenbossche, R. Walle, “Analysis of the Local Material Degradation Near Cutting Edges of Electrical Steel Sheets, IEEE Transaction on Magnetics, vol.44, No.11, 2008.

[33] G. Loisos, A.J. Moses, “Effect of mechanical and Nd:YAG laser cutting on magnetic ?ux distribution near the cut edge of non-oriented steels", *Journal of Materials Processing Technology*, Vol. 161, pp. 151-155, 2005.

[34] G. Loisos, A. J. Moses, “Critical Evaluation and Limitations of Localized Flux Density Measurements in Electrical Steels", *IEEE Transactions on Magnetics*, Vol. 37, No. 4, July 2001.

[35] C. Grünzweig, C. Davis, O. Bunk, M. Dierolf, G. Frei, and G. Kühne, “Neutron decoherence imaging for visualizing bulk magnetic domain structures", *Physical Review Letters*, Vol. 101, No. 2, pp. 025504-1-025504-9, 2008.

[36] A. Saleem, N. Alatawneh, R.R. Chromik, D.A. Lowther, “Effect of Shear Cutting on Microstructure and Magnetic Properties of Non-Oriented Electrical Steel", *IEEE Transaction on Magnetics*, Vol. 52, No. 5, 2016.

[37] H. Naumoski, B. Riedmüller,A. Minkow, U. Herr, “Investigation of the influence of different cutting procedures on the global and local magnetic properties of non-oriented electrical steel", *Journal of Magnetism and Magnetic Materials*, Vol. 392, pp. 126-133, 2015.

[38] R. Siebert,A. Wetzig,E. Beyer,B. Betz, “Localized investigation of magnetic bulk property deterioration of electrical steel", *Electric Drives Production Conference (EDPC)*, pp. 1-5, 2013.

[39] M. Bali, H. De Gersem, A. Muetze, “Determination of Original Non-Degraded and Fully Degraded Magnetic Properties of Material Subjected to Mechanical Cutting", *IEEE Transactions on Industry Applications*, January 2016.

[40] Y. Kurosaki, H. Mogi, H. Fujii, T. Kubota, M. Shiozaki, “Importance of punching and workability in non-oriented electrical steel sheets", *Journal of Magnetism and Magnetic Materials*, Vol. 320, 2008.

[41] H. M. S. Harstick, M. Ritter, W. Riehemann, “Influence of Punching and Tool Wear on the Magnetic Properties of Nonoriented Electrical Steel", *IEEE Transactions on Magnetics*, vol. 50, No. 4, April 2014.

[42] W. M. Arshad, T. Ryckebush, A. Broddefalk, F. Magnussen, H. Lendenmann, M. Lindenmo, “Characterization of electrical steel grades for direct application to electrical machine design tools", *Journal of Magnetism and Magnetic Materials*, Vol. 320, pp. 2538-2541, 2008.

[43] V. Manescu, G. Paltanea, H. Gavrila, I. Peter, “The Influence of Punching and Laser Cutting Technologies on the Magnetic Properties of Non-oriented Silicon Iron Steels", *International Symposium on Fundamentals of Electrical Engineering University Politehnica of Bucharest*, Nov. 2014.

[44] N. Takahashi, H. Morimoto, Y. Yunoki, D. Miyagi, “Effect of shrink ?tting and cutting on iron loss of permanent magnet motor", *Journal of Magnetism and Magnetic Materials*, Vol. 320, pp. e925-e928, 2008.

[45] R. Siebert, A. Wetzig, B. Betz, C. Grünzweig, E. Lehmann, E. Beyer, “Localized investigation of magnetic bulk property deterioration of electrical steel", *Electric Drives Production Conference (EDPC), 2013 3rd International*, pp. 1-5, Oct. 2013.

[46] A. Boglietti, “A First Approach for the Iron Losses Building Factor Determination", *IEEE Industry Applications Conference*, Vol. 1, Oct. 1999.

[47] Z. Gmyrek, A. Cavagnino, “Analytical Method for Determining the Damaged Area Width in Magnetic Materials Due to Punching Process", *IECON 2011 - 37th Annual Conference on IEEE Industrial Electronics Society*, Nov. 2011.

[48] H. Naumoski, D. Ulm, A. Maucher, L. Vandenbossche, S. Jacobs, “Magneto-optical and field-metric evaluation of the punching effect on magnetic properties of electrical steels with varying alloying content and grain size", *Electric Drives Production Conference (EDPC), 2014 4th International*, Oct. 2014.

[49] F. Ossart, E. Hug, O. Hubert, C. Buvat, R. Billardon, “Effect of Punching on Electrical Steels: Experimental and Numerical Coupled Analysis", *IEEE Transactions on Magnetics*, Vol. 36, No. 5, Sept. 2000.

[50] A. Kedous-Lebouc, B. Cornut, J.C. Perrier, Ph. Manfé, Th. Chevalier, “Punching in?uence on magnetic properties of the stator teeth of an induction motor", *Journal of Magnetism and Magnetic Materials*, Vol. 254-255, 2003.

[51] Yujing Liu, Kashif S. K., Sohail A. M., “Engineering considerations on additional iron losses due to rotational fields and sheet cutting", *Proceedings of the 2008 International Conference on Electrical Machines*, 2008.

[52] M. Akroune, R. Aouli, M.A. Dami, A. Mouillet, “Characterisation of nonoriented electric alloys under nonconventional conditions", *IEE Proceedings - Science, Measurement and Technology*, Vol. 143, Jan. 1996.

[53] W. M. Arshad, T. Ryckebush, F. Magnussen, H. Lendenmann, “Incorporating lamination processing and component manufacturing in electrical machine design tools", *Industry Applications Conference, 2007. 42nd IAS Annual Meeting. Conference Record of the 2007 IEEE*, Sept. 2007.

[54] E.G. Araujo, J. Schneider, K. Verbeken, G. Pasquarella, Y. Houbaert, “Dimensional Effects on Magnetic Properties of Fe?Si Steels Due to Laser and Mechanical Cutting", *IEEE Transactions on Magnetics*, Vol. 46, No. 2, Feb. 2010.

[55] Wenmin S., Jing L., Changyi L., “Effect of Cutting Techniques on the Structure and Magnetic Properties of a High-grade Non-oriented Electrical Steel", *Journal of Wuhan University of Technology-Mater. Sci. Ed.*, Vol. 29, Dec. 2014.

[56] P. Baudouin, M. De Wulf, L. Kestens, Y. Houbaert, “The effect of the guillotine clearance on the magnetic properties of electrical steels", *Journal of Magnetism and Magnetic Materials*, Vol. 256, pp.32-40, 2003.

[57] S. Steentjes, G. von P?ngsten, K. Hameyer, “An Application-Oriented Approach for Consideration of Material Degradation Effects Due to Cutting on Iron Losses and Magnetizability", *IEEE Transactions on Magnetics*, Vol. 50, No. 11, Nov. 2014.

[58] Hiroaki Toda, “Iron Loss Deterioration by Shearing Process in Non-Oriented Electrical Steel with Different Thicknesses", *IEEE Journal of Industry Applications*, Vol. 3, No. 1, pp. 55-61, 2014.

[59] A.J. Moses, N. Derebasi, G. Loisos, A. Schoppa, “Aspects of the cut-edge effect stress on the power loss and fux density distribution in electrical steel sheets", *Journal of Magnetism and Magnetic Materials*, Vol. 215-216, 2000.

[60] P. Baudouin, A. Belhadj, F. Breaban, A. Deffontaine, Y. Houbaert, “Effects of Laser and Mechanical Cutting Modes on the Magnetic Properties of Low and Medium Si Content Nonoriented Electrical Steels", *IEEE Transactions on Magnetics*, Vol. 38, No.5, Sep. 2002.

[61] R. Siebert, M. Lutke, A. Wetzig, E. Beyer, “Experimental findings on high power laser cutting of non-oriented electrical steel", *International Conference Magnetism and Metallurgy WMM'12*, Vol. 5, June 2012.

[62] R. Rygal, A.J. Moses, N. Derebasi, J. Schneider, A. Schoppa, “Infuence of cutting stress on magnetic feld and fux density distribution in non-oriented electrical steels", *Journal of Magnetism and Magnetic Materials*, Vol. 215-216, 2000.

[63] T. Nakata, M. Nakano, K. Kawahara, “Effects of Stress Due to Cutting on Magnetic Characteristics of Silicon Steel", *IEEE Translation Journal on Magnetics*, Vol. 7, No. 6, June 1992.

[64] Y. Kashiwara, H. Fujimura, K. Okamura, K. Imanishi, H. Yashiki, “Estimation Model for Magnetic Properties of Stamped Electrical Steel Sheet", *Electrical Engineering in Japan*, Vol. 183, No. 2, 2013.

[65] R. Rygal, A.J. Moses, N. Derebasi, J. Schneider, A. Schoppa, “Influence of cutting stress on magnetic field and flux density distribution in non-oriented electrical steels", *Journal of Magnetism and Magnetic Materials*, Vol. 215-216, 2000.

[66] M. Bali, A. Muetze, “Influences of CO2 Laser, FKL Laser, and Mechanical Cutting on the Magnetic Properties of Electrical Steel Sheets", *IEEE Transactions on Industry Applications*, Vol. 51, No. 6, Dec. 2015.

[67] A. Belhadj, P. Baudouin, F. Breaban, A. Deffontaine, M. Dewulf, Y. Houbaert, “Effect of laser cutting on microstructure and on magnetic properties of grain non-oriented electrical steels", *Journal of Magnetism and Magnetic Materials*, Vol. 256, 2003.

[68] A. Belhadj, P. Baudouin, Y. Houbaert, “Simulation of the HAZ and magnetic properties of laser cut non-oriented electrical steels", *Journal of Magnetism and Magnetic Materials*, Vol. 248, pp. 34-44, 2002.

[69] M. Emura, F.J.G. Landgraf, W. Ross, J.R. Barreta, “The in?uence of cutting technique on the magnetic properties of electrical steels", *Journal of Magnetism and Magnetic Materials*, Vol. 254-255, pp. 358-360, 2003.

[70] P. Lazari, K. Atallah, J. Wang, “Effect of Laser Cut on the Performance of Permanent Magnet Assisted Synchronous Reluctance Machines", *IEEE Transactions on Magnetics*, Vol. 51, No. 11, Nov. 2015.

[71] V. Manescu, G. Paltanea, H. Gavrila, “Some Important Effects of the Water Jet and Laser Cutting Methods on the Magnetic Properties of the Non-oriented Silicon Iron Sheets", *The 9^{th} International Symposium on Advanced Topics in Electrical Engineering*, 2015.

[72] A. Schoppa, H. Louis, F. Pude, Ch. von Rad, “In?uence of abrasive waterjet cutting on the magnetic properties of non-oriented electrical steels", *Journal of Magnetism and Magnetic Materials*, Vol. 254-255, 2003.

[73] A. Schoppa, J. Schneider, C.D. Wuppermann, “Infuence of the manufacturing process on the magnetic properties of non-oriented electrical steels", *Journal of Magnetism and Magnetic Materials*, Vol. 215-216, pp. 74-78, 2000.

[74] M. Bali, H. De Gersem, A. Muetze, “Finite-Element Modeling of Magnetic Material Degradation Due to Punching", *IEEE Transactions on Industry Applications*, Vol. 50, No. 2, Feb. 2014.

[75] A. Arkkio, “Analysis of Induction Motors Based on the Numerical Solution of the Magnetic Field and Circuit Equations", *Electrical Engineering Series*, No. 59, 1987.

A Mechanical Cutting

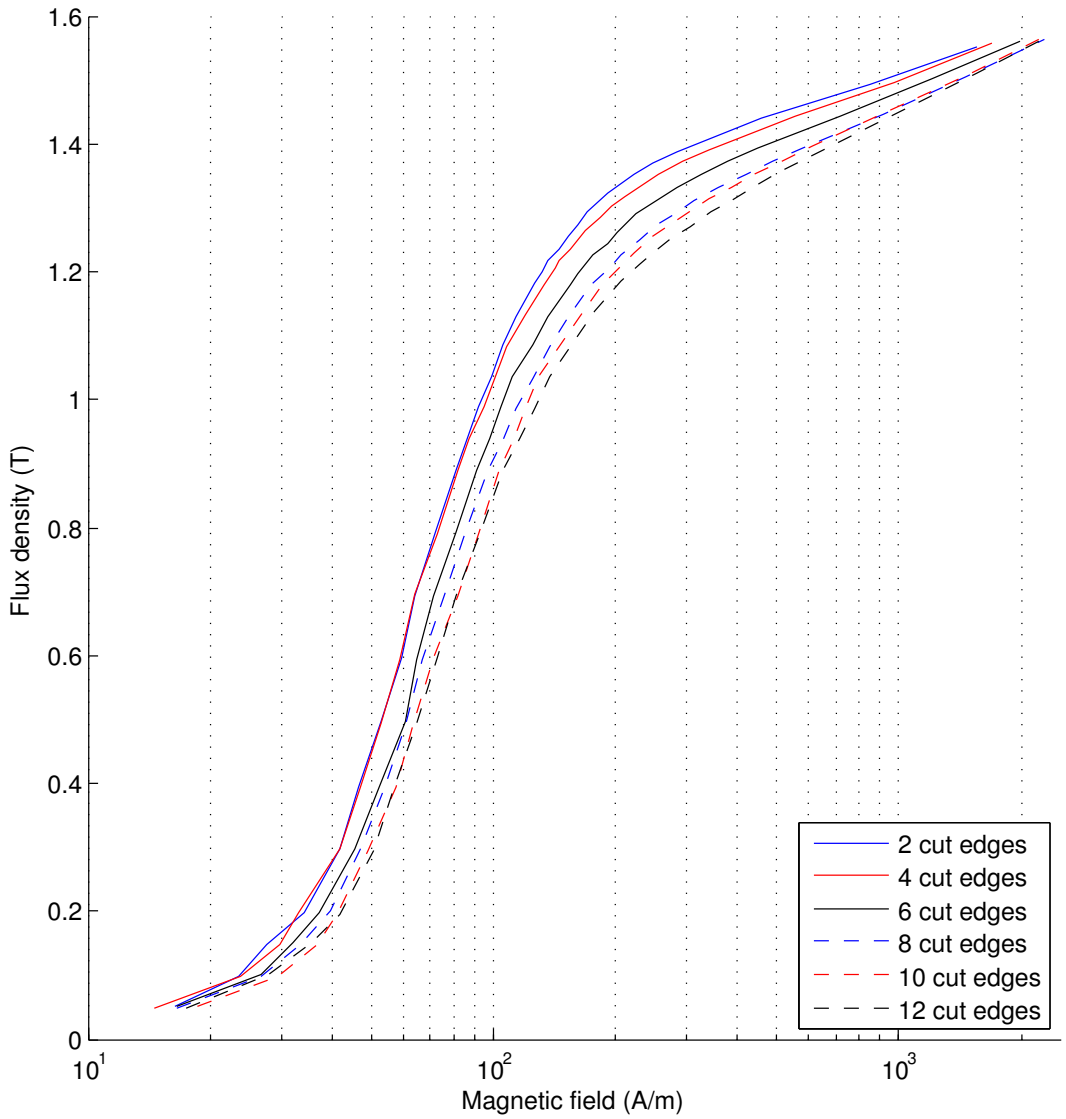

Figure A1: Magnetization curves at 50 Hz for mechanical cutting. All the configurations of the strips are reported.

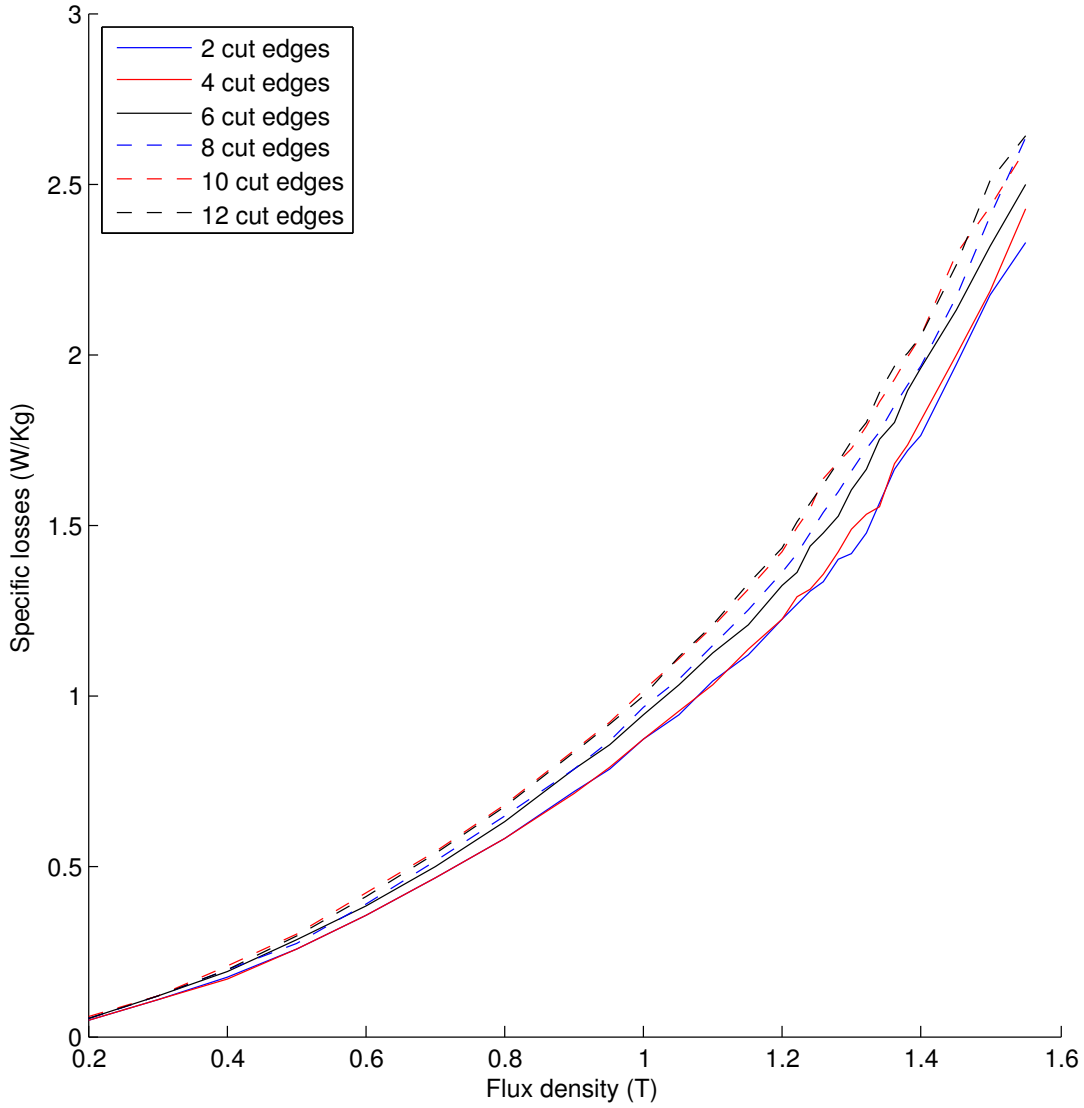

Figure A2: Specific losses at 50 Hz for mechanical cutting. All the configurations of the strips are reported.

B Laser Cutting

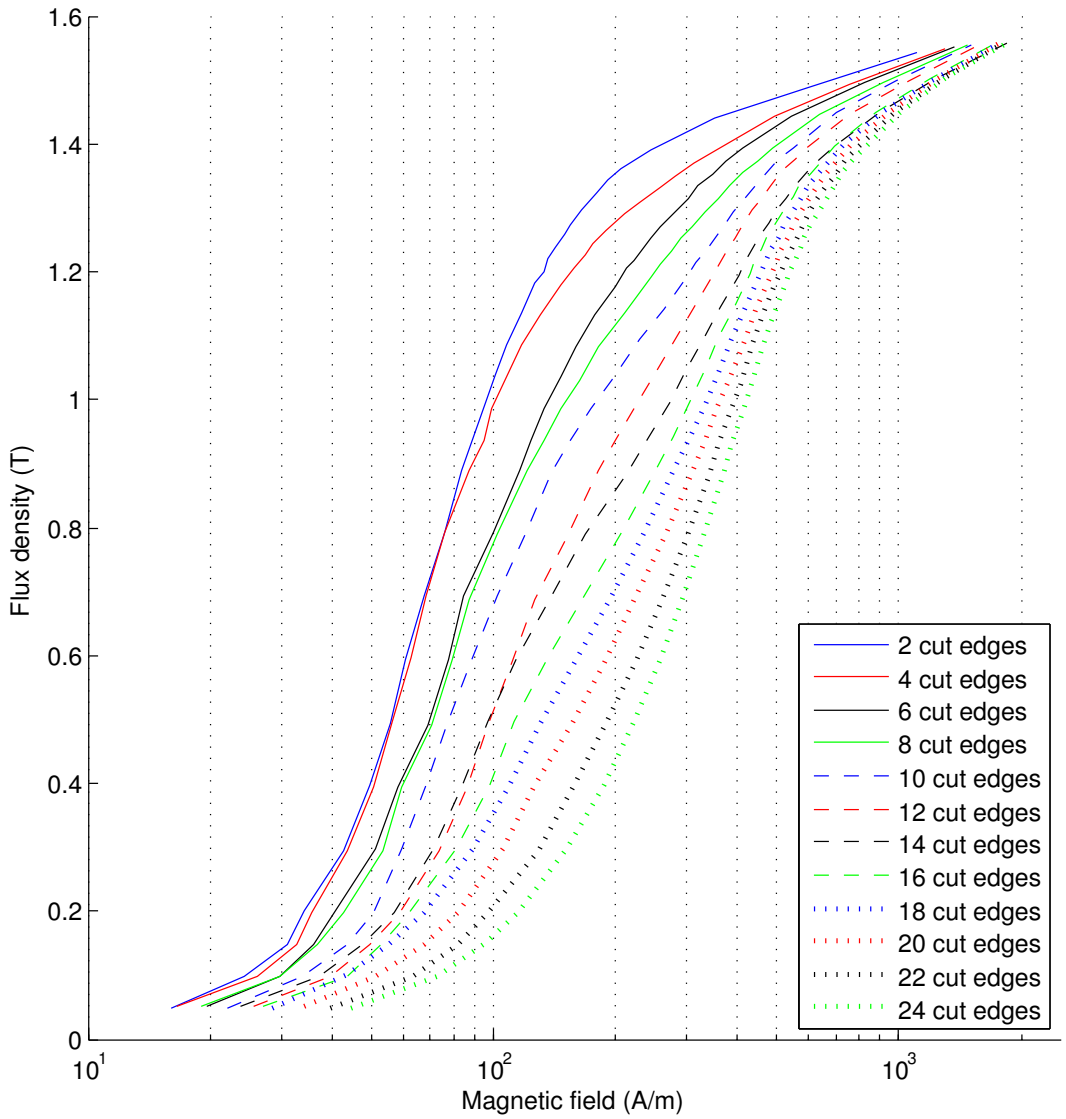

Figure B1: Magnetization curves at 50 Hz for laser cutting. All the configurations of the strips are reported.

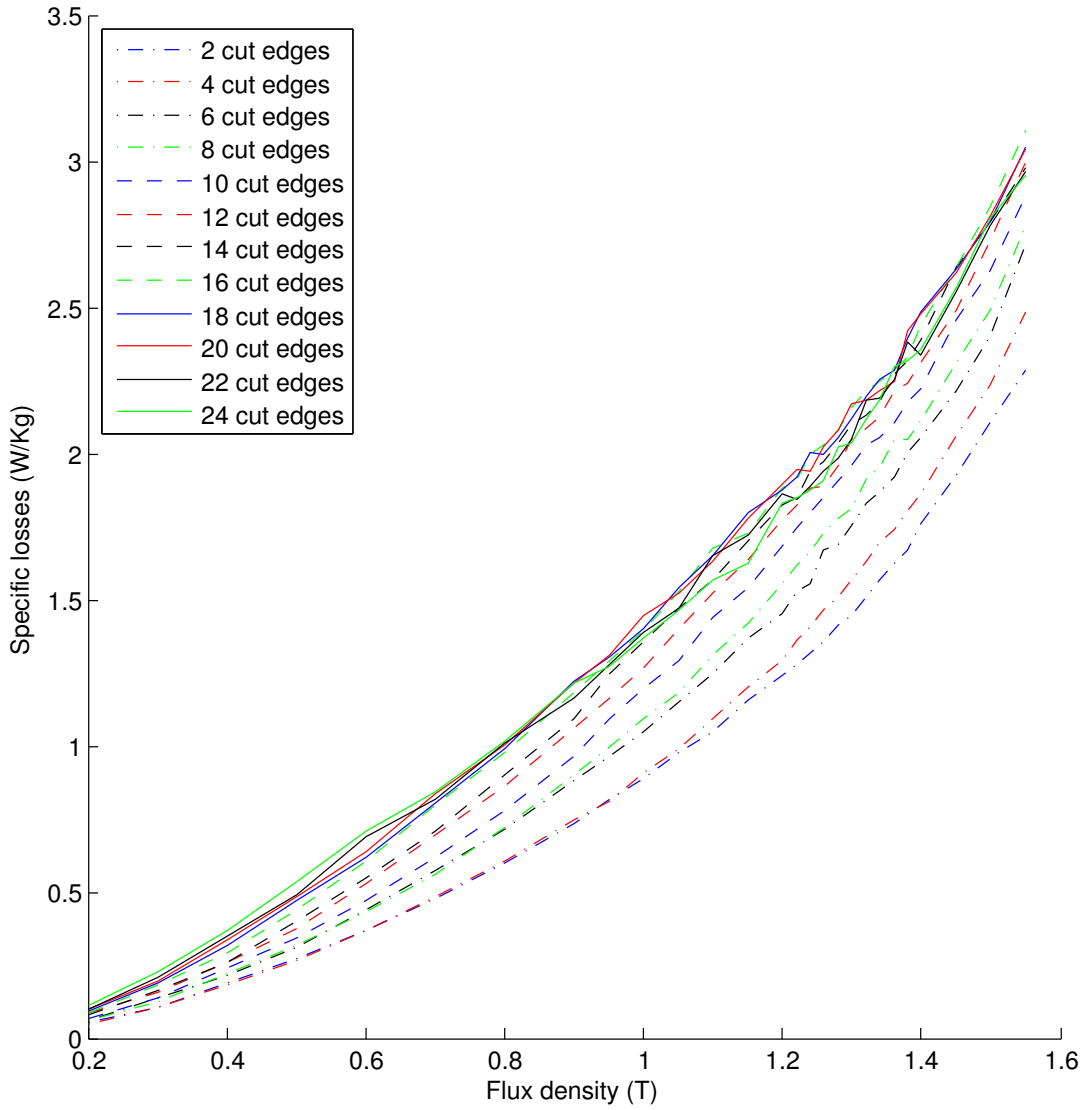

Figure B2: Specific losses at 50 Hz for laser cutting. All the configurations of the strips are reported.